


## RESEARCH ARTICLE

# P2X<sub>7</sub> receptor-dependent increase in endocannabinoid 2-arachidonoyl glycerol production by neuronal cells in culture: Dynamics and mechanism

Simar Singh<sup>1</sup>  | Dennis Sarroza<sup>1</sup> | Anthony English<sup>1</sup> | Dale Whittington<sup>2</sup> |  
 Ao Dong<sup>3</sup> | Michael Malamas<sup>4</sup> | Alexandros Makriyannis<sup>4</sup> | Mario van der Stelt<sup>5</sup> |  
 Yulong Li<sup>3</sup> | Larry Zweifel<sup>1,6,7,8</sup> | Michael R. Bruchas<sup>1,7,8,9</sup> |  
 Benjamin B. Land<sup>1,7,8</sup> | Nephi Stella<sup>1,6,7,8</sup>

<sup>1</sup>Department of Pharmacology, University of Washington, Seattle, Washington, USA

<sup>2</sup>Department of Medicinal Chemistry, University of Washington, Seattle, Washington, USA

<sup>3</sup>Peking University School of Life Sciences, PKU-IDG/McGovern Institute for Brain Research, Peking-Tsinghua Center for Life Sciences, Academy for Advanced Interdisciplinary Studies, Peking University, Beijing, China

<sup>4</sup>Center for Drug Discovery and Departments of Chemistry and Chemical Biology and Pharmaceutical Sciences, Northeastern University, Boston, Massachusetts, USA

<sup>5</sup>Leiden Institute of Chemistry, Leiden University, Leiden, Netherlands

<sup>6</sup>Department of Psychiatry and Behavioral Sciences, University of Washington, Seattle, Washington, USA

<sup>7</sup>Center for Cannabis Research, University of Washington, Seattle, Washington, USA

<sup>8</sup>Center for the Neurobiology of Addiction, Pain, and Emotion, University of Washington, Seattle, Washington, USA

<sup>9</sup>Department of Anesthesiology and Pain Medicine, University of Washington, Seattle, Washington, USA

## Correspondence

Nephi Stella, Center for the Neurobiology of Addiction, Pain, and Emotion, University of Washington, Seattle, Washington, USA.  
 Email: [nstella@uw.edu](mailto:nstella@uw.edu)

## Funding information

Science Fund for Creative Research Groups of the National Natural Science Foundation of China, Grant/Award Number: 81821092; Shenzhen-Hong Kong Institute of Brain Science, Grant/Award Number: NYKFKT2019013; Beijing Municipal Science & Technology Commission, Grant/Award Numbers: Z181100001318002, Z181100001518004; National Natural Science Foundation of China, Grant/Award Numbers: 31871087, 31925017; National Institutes of Health, Grant/Award Numbers: DA033396, DA047626, DA055448, NS118130, T32GM007750; University of Washington Center of Excellence in Opioid Addiction Research/Molecular Genetics Resource Core, Grant/Award Number: P30DA048736; NIH BRAIN Initiative, Grant/Award Number: 1U01NS113358; Peking-Tsinghua Center for

**Background and Purpose:** Neurotransmission and neuroinflammation are controlled by local increases in both extracellular ATP and the endocannabinoid 2-arachidonoyl glycerol (2-AG). While it is known that extracellular ATP stimulates 2-AG production in cells in culture, the dynamics and molecular mechanisms that underlie this response remain poorly understood. Detection of real-time changes in eCB levels with the genetically encoded sensor, GRAB<sub>eCB2.0</sub>, can address this shortfall.

**Experimental Approach:** 2-AG and arachidonylethanolamide (AEA) levels in Neuro2a (N2a) cells were measured by LC-MS, and GRAB<sub>eCB2.0</sub> fluorescence changes were detected using live-cell confocal microscopy and a 96-well fluorescence plate reader.

**Key Results:** 2-AG and AEA increased GRAB<sub>eCB2.0</sub> fluorescence in N2a cells with EC<sub>50</sub> values of 81 and 58 nM, respectively; both responses were reduced by the cannabinoid receptor type 1 (CB<sub>1</sub>R) antagonist SR141617 and absent in cells expressing the mutant-GRAB<sub>eCB2.0</sub>. ATP increased only 2-AG levels in N2a cells, as measured by LC-MS, and induced a transient increase in the GRAB<sub>eCB2.0</sub> signal within minutes primarily via activation of P2X<sub>7</sub> receptors (P2X<sub>7</sub>R). This response was dependent on diacylglycerol lipase β activity, partially dependent on extracellular calcium and

**Abbreviations:** 2-AG, 2-arachidonoyl glycerol; ABHD6, α/β-hydrolase domain containing 6; ABPP, activity-based protein profiling; AEA, arachidonylethanolamide; AR-C, AR-C118925; AM4113, CB<sub>1</sub> receptor antagonist; cpGFP, circularly permuted-green fluorescent protein; CP, CP55940; DO34, diacylglycerol lipase inhibitor; DAGL, diacylglycerol lipase; GRAB<sub>eCB2.0</sub>, endocannabinoid sensor; MAGL, monoacylglycerol lipase; SR1, SR141617; U73122, phospholipase C inhibitor.

Life Sciences; State Key Laboratory of Membrane Biology at Peking University School of Life Sciences

[Correction added on 15 April 2024, after first online publication: Figures 1 and 3 has been corrected in this version.]

phospholipase C activity, but not controlled by the 2-AG hydrolysing enzyme,  $\alpha/\beta$ -hydrolase domain containing 6 (ABHD6).

**Conclusions and Implications:** Considering that P2X<sub>7</sub>R activation increases 2-AG levels within minutes, our results show how these molecular components are mechanistically linked. The specific molecular components in these signalling systems represent potential therapeutic targets for the treatment of neurological diseases, such as chronic pain, that involve dysregulated neurotransmission and neuroinflammation.

#### KEYWORDS

2-AG, ATP, endocannabinoids, genetically encoded sensor, purinergic receptors

## 1 | INTRODUCTION

Increases in the extracellular concentration of **ATP** and activation of purinergic receptors modulate multiple physiological processes, including neurotransmission and neuroinflammation (Rodrigues et al., 2015). Specifically, increases in the extracellular ATP concentration may result from neuronal depolarization, which releases ATP through vesicular and channel-dependent mechanisms mediated by **connexins and pannexins**, or from dying cells with disrupted plasma membranes that release intracellular ATP (Grygorczyk et al., 2021; Rodrigues et al., 2015). Extracellular ATP activates a subset of the P2 purinergic receptors, encompassing eight metabotropic **P2Y receptors** and seven ligand-gated **P2X ion channels**, which are differentially expressed by neighbouring neuronal and immune cells (Kennedy, 2021). **P2X<sub>7</sub>R**s are calcium-permeable channels and the only P2 receptor subtype activated by high micromolar-to-millimolar concentrations of ATP (Chavez-Noriega et al., 1997; North & Surprenant, 2000). Activation of P2X<sub>7</sub>R leads to the opening of its pore and a rapid increase in intracellular calcium concentrations [ $\text{Ca}^{2+}$ ]<sub>i</sub>, which activates multiple downstream calcium-dependent effectors, such as **phospholipase C** (PLC), **phospholipase A<sub>2</sub>**, **phospholipase D**, **sphingomyelinases**, **kinases**, and **caspases** (Kopp et al., 2019). Multiple studies have explored the role and mechanism of P2X<sub>7</sub>R signalling in the pathogenesis of neurological diseases, such as chronic pain, and have shown that it represents a promising therapeutic target (Andrejew et al., 2020; Ren & Illes, 2022).

One of the signalling pathways implicated in chronic pain and stimulated by increases in extracellular ATP is the **endocannabinoid** (eCB) signalling system. eCB signalling plays a fundamental role in the control of neurotransmission and neuroinflammation, and its molecular components have been targeted for the treatment of multiple neurological diseases (Lu & Mackie, 2021). For example, eCB levels are increased in rodent models of neuropathic pain (Mitrirattanakul et al., 2006), eCBs reduce both pronociceptive neurotransmission and the proinflammatory phenotype of immune cells (Tanaka et al., 2020). eCB activation of its receptors, including **CB<sub>1</sub>R** and **CB<sub>2</sub>R**, produces analgesia in multiple pain models (Baggelaar et al., 2018; Hossain et al., 2020). Accordingly, inhibitors of eCB inactivation and modulators of CB<sub>1</sub>R signalling reduce neuropathic pain in several mouse

### What is already known

- Extracellular ATP regulates neurotransmission and neuroinflammation.
- ATP stimulates 2-AG production in microglia and astrocytes by a yet to be described mechanism.

### What does this study add

- ATP and BzATP differentially increased 2-AG levels in Neuro2a cells through a P2X<sub>7</sub> receptor-dependent mechanism.

### What is the clinical significance

- Our results show how ATP signalling can increase 2-AG levels in cultured neurons.
- The purinergic and endocannabinoid systems may represent potential therapeutic targets for treatment of neurological diseases.

models (Covelo et al., 2021; Lu & Mackie, 2021). The two best-studied eCBs, **AEA** and **2-AG**, differ in four key aspects: (1) they are produced by distinct biosynthetic pathways (**N-acyl phosphatidylethanolamine phospholipase D** (NAPE-PLD) vs. PLC and diacylglycerol lipase [DAGL], respectively); (2) 2-AG is 10- to 1000-fold more abundant than AEA in cells; (3) AEA is a high-affinity, partial agonist at CB<sub>1</sub>R, whereas 2-AG exhibits lower affinity at CB<sub>1</sub>R and acts as full agonist; and (4) AEA is mainly inactivated by **fatty acid amide hydrolase** (FAAH) whereas 2-AG is differentially inactivated by **monoacylglycerol lipase** (MAGL) and  **$\alpha\beta$ -hydrolase 6** (ABHD6) (Lu & Mackie, 2016; Zou & Kumar, 2018). Several important aspects of eCB signalling that remain unexplored include the dynamics of the

stimulated production of eCBs, the receptor subtypes and enzymes that control this activity-dependent production, and the dynamics of their on-off responses. These dynamic interactions may be crucial for fine tuning analgesic responses.

Genetically encoded fluorescent sensors allow for real-time detection of changes in the levels of select endogenously produced signalling molecules (Labouesse & Patriarchi, 2021). This technology leverages the high-affinity binding of endogenous molecules to specific **G protein-coupled receptors** (GPCRs), which stabilizes a conformation to elicit fluorescence of a circularly permuted-green fluorescent protein (cpGFP) introduced in the third intracellular loop of the GPCR (Ravotto et al., 2020). GRAB<sub>eCB2.0</sub>, a recently developed eCB sensor, detects changes in eCB levels with subsecond resolution, and its activation has been demonstrated in stimulated cells in culture and mouse brain slices, and mouse brain during behavioural studies (Dong et al., 2021; Farrell et al., 2021; Liput et al., 2022; Liu et al., 2022; Singh et al., 2023). Thus, leveraging the spatiotemporal properties of the GRAB<sub>eCB2.0</sub> provides an opportunity to study the dynamics and molecular mechanisms of eCB signalling at the cellular level.

We previously have shown that ATP increases 2-AG production in astrocytes and microglia cells in culture through the activation of P2X<sub>7</sub>R (Walter et al., 2004; Witting et al., 2004); however, the detailed mechanism and the dynamics of this response remains unknown. The mouse neuroblastoma cell line, N2a, expresses multiple subtypes of P2 receptors, as well as the molecular components involved in eCB signalling (e.g., lipases involved in eCB production and inactivation, and CB<sub>1</sub>R) and thus represents an ideal model system to study the molecular mechanism that link and control P2X<sub>7</sub>R-dependent increases in 2-AG production (Baggelaar et al., 2015; Hsu et al., 2012; Jung et al., 2011). Here, we characterized changes in GRAB<sub>eCB2.0</sub> signal when expressed by N2a cells in culture and determined the specific P2 receptor subtype, calcium-dependence, lipases, and dynamics that mediate ATP-dependent increases in endogenous 2-AG production in these neuroblastoma cells.

## 2 | METHODS

### 2.1. Materials

Adenosine 5'-triphosphate (Sigma), **A740003** (Tocris), 2-arachidonoylglycerol (Cayman), 1-arachidonoylglycerol (Cayman), **THC CP55940** (Cayman), **SR141716** (NIDA Drug Supply Program), arachidonylethanolamide (Cayman), **DO34** (AOBIOUS), AM12100 (gift from Dr. Alexander Makriyannis), **U73122 hydrate** (Sigma), 1,2-bis(2-aminophenoxy)ethane-N,N,N',N'-tetraacetate-acetoxymethyl ester (BAPTA-AM; Sigma), goat anti-CB<sub>1</sub>R c-terminal antibody (gift from Dr. Ken Mackie; 1:1000 for IF and 1:2500 for immunoblotting); AlexaFluor 647 conjugated donkey anti-goat (Invitrogen; 1:1000); and rabbit anti-actin (1:2500; Sigma Aldrich); IRDye 800 CW conjugates donkey anti-goat (LI-COR); IRDye 680 RD conjugated goat anti-rabbit (LI-COR).

### 2.2. Cloning

GRAB<sub>eCB2.0</sub> and mut-GRAB<sub>eCB2.0</sub> DNA were subcloned into an AM/CBA-WPRE-bGH plasmid as previously described (Singh et al., 2023) using an In-Fusion cloning system (Takara Bio Inc, Japan).

#### 2.1 | Cell culture

Neuro2a cells (gift from Dr. John Scott, **RRID:CVCL\_0470**) were grown in DMEM (Gibco, supplemented with 10% fetal bovine serum and 1% penicillin/streptomycin) at 37°C and 5% CO<sub>2</sub>. To passage cells for experiments, a confluent 10-cm plate of cells was detached by incubating with 0.25% Trypsin-EDTA for 2–3 min at 37°C. Then, 4–5 ml of supplemented DMEM was added, and gentle pipetting was used to remove any cells still attached. Finally, the cells were transferred to a new plate with fresh supplemented DMEM. Cells were passaged every 3–4 days and for no more than 25 passages.

#### 2.2 | Transfection

All transfections were done with polyethylenimine (PEI, 25K linear, Polysciences) as previously described (Singh et al., 2023). Cells were transfected when they were at least 50% confluent and were incubated for 24 h post-transfection before lysis (for western blotting), fixation (for immunofluorescence), or for use in GRAB<sub>eCB2.0</sub> fluorescence assays.

#### 2.3 | Immunofluorescence

All immunofluorescence experiments were conducted as previously described (Singh et al., 2023). Briefly, N2a cells were grown on glass coverslips (Fisher Scientific) coated with poly-D-lysine (50 ng·ml<sup>-1</sup>, Sigma, P6407), transfected with 0.75-μg DNA for 24 h, fixed with 4% paraformaldehyde in PBS (Alfa Aeser). To stain for GRAB<sub>eCB2.0</sub>, the fixed cells were permeabilized and blocked with 0.1% saponin (made fresh) and 1% bovine serum albumin (BSA, Sigma) made in PBS for 30 min at room temperature. Cells were then incubated primary antibody (goat anti-CB<sub>1</sub>R antibody 1:1000 overnight at 4°C), washed with PBS 6×, incubated in secondary antibody (AlexaFluor647 conjugated donkey anti-goat secondary antibody 1:1000, 1 h at room temperature; Invitrogen), washed with PBS 6×, air dried overnight, and mounted using ProLong Diamond Antifade Mountant with **DAPI** (ThermoFisher). All antibodies were diluted in 0.1% saponin and 1% BSA made in PBS. Cells were imaged with a Leica SP8X line scanning confocal microscope using a 40× oil objective lens.

#### 2.4 | Western blotting

N2a cells were plated at a density of 500,000 cells per well in a six-well plate and were transfected the following day with 0.75-μg DNA;

24 h after transfection, cells were harvested with a cell scraper, pelleted by centrifuging at  $500 \times g$  for 10 min, and cell pellets were kept at  $-80^{\circ}\text{C}$  until further use. To make cell lysates, cell pellets were thawed on ice, resuspended in lysis buffer (25-mM HEPES pH 7.4, 1-mM EDTA, 6-mM  $\text{MgCl}_2$ , and 0.5% CHAPS), Dounce homogenized on ice (20–30 strokes), incubated on a rotator at  $4^{\circ}\text{C}$  for 1 h, and then centrifuged at  $700 \times g$  for 10 min at  $4^{\circ}\text{C}$ . The supernatant was collected and its protein concentration was determined using a DC Protein Assay. Samples were then mixed with  $4 \times$  Laemmli Sample Buffer containing 10%  $\beta$ -mercaptoethanol and incubated at  $65^{\circ}\text{C}$  for 5 min; 25  $\mu\text{g}$  of protein were loaded onto a 10% polyacrylamide gel, transferred to PVDF membrane, and blocked with 5% BSA in TBS (1 h at room temperature). Western blot detection of GRAB<sub>eCB2.0</sub> was performed as previously described (Singh et al., 2023) using the following antibodies: (1) primary antibodies (incubated overnight at  $4^{\circ}\text{C}$ ): goat anti-CB<sub>1</sub>R primary (1:2500) and rabbit anti-actin (1:2500; Sigma Aldrich); (2) secondary antibodies (incubated for 1 h at room temperature): IRDye 800 CW conjugates donkey anti-goat (Licor) and IRDye 680 RD conjugated goat anti-rabbit (Licor).

## 2.5 | N2a membrane proteome preparation

Cells were washed twice by adding ice cold Dulbecco's phosphate buffered saline to attached cells and aspirating and then harvested by adding 1 ml of ice cold dPBS and detaching cells with a cell scraper and pelleted by centrifuging at  $500 \times g$  for 10 min. The supernatant was discarded, and the pellets were stored at  $-80^{\circ}\text{C}$  until further use. To isolate the membrane proteome of the cells, the cell pellets were thawed on ice, resuspended in lysis buffer (20-mM HEPES pH 7.2, 2-mM DTT, 10  $\text{U}\cdot\text{ml}^{-1}$  Benzonase), Dounce homogenized with 20–30 strokes, and centrifuged at  $100,000 \times g$  for 45 min (Beckman coulter rotor Ti55). The supernatant was discarded, and the pellet was resuspended in buffer (20-mM HEPES pH 7.2 and 2-mM DTT). Protein concentrations of samples were determined (DC protein assay, Biorad) before aliquoting and flash freezing samples in liquid nitrogen. Samples were stored at  $-80$  until use.

## 2.6 | Brain tissue membrane proteome preparation

Adult wild type C57BL/6 mice were decapitated, cortical brain tissue harvested, flash frozen in liquid nitrogen, and stored at  $-80^{\circ}\text{C}$ . To prepare membrane proteome, the tissue was thawed on ice, Dounce homogenized in ice-cold lysis buffer (20 mM HEPES pH 7.2, 2 mM DTT, 10  $\text{U}\cdot\text{ml}^{-1}$  Benzonase) with 20–30 strokes, centrifuged at ( $2500 \times g$ , 3 min, and  $4^{\circ}\text{C}$ ) to pellet cell debris. The supernatant was then centrifuged at  $100,000 \times g$  for 45 min (Beckman coulter rotor Ti55). The pellet was resuspended in buffer (20-mM HEPES pH 7.2 and 2-mM DTT). Protein concentrations of samples were determined (DC protein assay, Biorad) before aliquoting and flash freezing samples in liquid nitrogen. Samples were stored at  $-80$  until use.

## 2.7 | Live-cell imaging

Glass bottom cell culture plates (MatTek) were coated with poly-D-lysine (50  $\text{ng}\cdot\text{ml}^{-1}$ , Sigma) for 1–2 h at  $37^{\circ}\text{C}$ , after which the poly-D-lysine was removed, and coverslips were washed three times with sterile water and one time with DMEM. N2a cells were detached and resuspended in supplemented DMEM as described above, counted using a haemocytometer, plated (250,000 cells per well) and were transfected after 24 h with 0.75  $\mu\text{g}$  DNA; 24 hours after transfection, the growth media was exchanged for serum-free DMEM and cells were incubated at  $37^{\circ}\text{C}$  and 5%  $\text{CO}_2$  for 1–2 h. To image, the serum-free DMEM was exchanged for room temperature phosphate-buffered saline containing 1-mM  $\text{CaCl}_2$  and 0.55-mM  $\text{MgCl}_2$ . The plates were transferred to a line-scanning, confocal microscope (Leica SP8X), and cells were imaged using a  $40 \times$  oil objective with the following settings: 485 excitation and 525 emission wavelength, 5% laser power, HyD hybrid detector, and a scan speed of 200 lines Hz (0.388 frames per second) with bidirectional scanning. All treatments were made in 1  $\text{mg}\cdot\text{ml}^{-1}$  BSA in PBS and added directly to buffer for a final concentration of 0.1  $\text{mg}\cdot\text{ml}^{-1}$  BSA.

## 2.8 | Gel-based activity-based protein profiling

Membrane proteome was thawed on ice, and 10  $\mu\text{g}$  of protein was used for assay with volume normalized using 20-mM HEPES. Protein was incubated with activity-based probes, either 250-nM ActivX TAMRA-FP (ThermoFisher Scientific) or 2- $\mu\text{M}$  MB064 (gift from Dr. Mario van der Stelt) for 15 min at  $37^{\circ}\text{C}$ . Reaction was quenched with  $4 \times$  Laemmli sample buffer with 10%  $\beta$ -mercaptoethanol (BioRad) and run on a 10% polyacrylamide gel (Biorad). After running for about 1 h at 150 mV, the gel was removed from the casing. Fluorescence was detected using a Chemidoc MP (Biorad) using a Cy3, green epifluorescence filter (605/50) for the activity-based probe and Cy5, red epifluorescence filter (695/55) for the protein ladder. The gel was then stained with Coomassie Brilliant Blue (0.1% Coomassie brilliant blue R-250, 25% glacial acetic acid, 40% ethanol) to obtain total protein.

## 2.9 | Ninety-six-well plate reader GRAB<sub>eCB2.0</sub> detection

Clear-bottom, black 96-well plates (USA Scientific 5665-5087) were coated with poly-D-lysine (50  $\text{ng}\cdot\text{ml}^{-1}$ , Sigma, P6407) for 1–2 h at  $37^{\circ}\text{C}$ , after which the poly-D-lysine was removed, and coverslips were washed three times with sterile water and one time with DMEM. N2a cells were detached and resuspended in supplemented DMEM as described above, counted using a haemocytometer, and then plated (20,000 cells per well) and were transfected after 24 h with 0.1- $\mu\text{g}$  DNA and 0.3  $\mu\text{g}$  of PEI in 10  $\mu\text{l}$  of serum-free DMEM; 24 h after transfection, growth media was initially replaced with

serum-free DMEM for 1 h (with or without ABHD6 and DAGL inhibitors), before replacing with PBS supplemented with 1-mM  $\text{CaCl}_2$  and 0.55-mM  $\text{MgCl}_2$ . Cells were incubated at room temperature for 20 min, and then a 1-min baseline fluorescence reading was obtained using a fluorescence plate reader using 485 excitation and 525 emission filter settings with a 515-nm cutoff, and a speed of one reading every 20 s. Immediately after baseline reading, treatments (made in 1 mg·ml<sup>-1</sup> BSA and PBS) were added to buffer in wells. Approximately 2 min after the addition of treatment, the plate was read with the same filter settings for 30 min. For cells pretreated with SR1, SR1 made in PBS was added to cells after media had been replaced with PBS and incubated for 20 min before baseline reading.

## 2.10 | LC-MS/MS

When N2A cells reached 90%–100% confluency, the growth media was removed and replaced with serum-free DMEM. Cells were incubated for 1 h at 37°C, after which the media was replaced with PBS supplemented with 1-mM  $\text{CaCl}_2$  and 0.55-mM  $\text{MgCl}_2$ , incubated at room temperature for about 10 min and then treated for 2 or 10 min. Reaction was quenched by removing buffer and washing three times with ice cold PBS before scraping cells off and centrifuging at 500 × *g* for 10 min at 4°C to pellet the cells. The buffer was then aspirated, and the pellet resuspended in 20 ml of 0.02% trifluoroacetic acid and 100-ml acetonitrile with 1 picomole of 2-AG-d<sup>5</sup> internal standard (Cayman Chemical) on ice before transferring to 2.5 ml of acetonitrile in a glass vial. Samples were briefly vortexed and incubated overnight at -20°C. After the overnight incubation, the homogenate was centrifuged at 2000 × *g* for 5 min to remove debris, the supernatant was collected and evaporated under nitrogen stream at 35°C and then resuspended in 50 μl of acetonitrile. The samples were capped under nitrogen stream and stored at -80°C until ready for the LC-MS/MS. Chromatographic separation was achieved using a Zorbax C18, 2.1 × 50 mm, 3.5 μm reverse-phase column (Agilent). The HPLC output was directed into the electrospray ionization source of a Waters Xevo TQ-S mass spectrometer. Ionization was done in positive mode to detect 2-AG and AEA and in negative mode to detect arachidonic acid. All experiments were done in duplicate; results from each technical replicate were averaged and plotted using GraphPad Prism.

## 2.11 | Animals

Wild type C57BL/6 mice were bred on site. All animal care and use conformed to the National Institutes of Health Guide for Care and Use of Laboratory Mice and was approved by the University of Washington Institutional Animal Care and Use Committee. Animal studies are reported in compliance with the ARRIVE guidelines (Percie du Sert et al., 2020) and with the recommendations made by the British Journal of Pharmacology (Lilley et al., 2020).

## 2.12 | Data analysis

The  $\Delta F/F_0$  fold-change of the GRAB<sub>eCB2.0</sub> fluorescent signal was calculated by either FIJI ImageJ (for live cell confocal microscopy) or MATLAB (for the 96-well plate fluorescence assay) as previously described (Singh et al., 2023). To analyse live-cell microscopy data, changes in GRAB<sub>eCB2.0</sub> fluorescent signals were calculated by first averaging each cell's baseline fluorescence ( $F_0$ : fluorescent signal averaged over 30 s approximately 30 s prior to start of agonist treatment) and then calculating fold-change in fluorescent signal ( $\Delta F/F_0$ : subtracting the signal at any post-agonist time of interest). To analyse the 96-well plate assay data: changes in GRAB<sub>eCB2.0</sub> signal were calculated by averaging baseline fluorescence for each well ( $F_0$ : average fluorescent signal over 1-min basal reading, about 2 min before agonist treatment) and calculating relative fold-change in fluorescent signal ( $\Delta F/F_0$ ) by subtracting the signal at every time point measured (to construct a time course) or at a specific time point (i.e., relative change 1 min post-treatment) by  $F_0$  and then dividing by  $F_0$ . Every condition was tested in triplicate, so the results represent the average  $\Delta F/F_0$  values for each set of technical replicates. GRAB<sub>eCB2.0</sub> activation was determined by calculating  $\Delta\Delta F/F_0$  between specific time points (i.e., subtracting the  $\Delta F/F_0$  at time = 0 and  $\Delta F/F_0$  at time at maximum signal). To analyse data generated by the 96-well plate reader, we developed a MATLAB R2021a algorithm (available at <https://github.com/StellaLab/StellaLab.git>) that averages the fluorescent signal value of each well over time, for multiple experiments and at select timepoints. Data are shown as mean ± SEM and significance was determined by running a two-way ANOVA with Dunnett's multiple comparison test using GraphPad Prism. This study complies with the recommendations of the British Journal of Pharmacology on experimental design and analysis (Curtis et al., 2022). Statistical significance was defined as a P-value < 0.05 and indicated by a single asterisk (\*).

## 2.13 | Nomenclature of targets and ligands

Key protein targets and ligands in this article are hyperlinked to corresponding entries in <http://www.guidetopharmacology.org>, and are permanently archived in the Concise Guide to PHARMACOLOGY 2023/24 (Alexander, Christopoulos, et al., 2023; Alexander, Fabbro, et al., 2023; Alexander, Mathie, et al., 2023).

## 3 | RESULTS

### 3.1 | Real-time change in GRAB<sub>eCB2.0</sub> fluorescent signal in N2a cells

To drive robust GRAB<sub>eCB2.0</sub> expression, we transfected N2a cells in culture with plasmids containing the chimeric cytomegalovirus-chicken β-actin promoter and eCB2.0 (Figure 1a). Figure 1b shows robust GRAB<sub>eCB2.0</sub> expression 24 h after transfection detected by

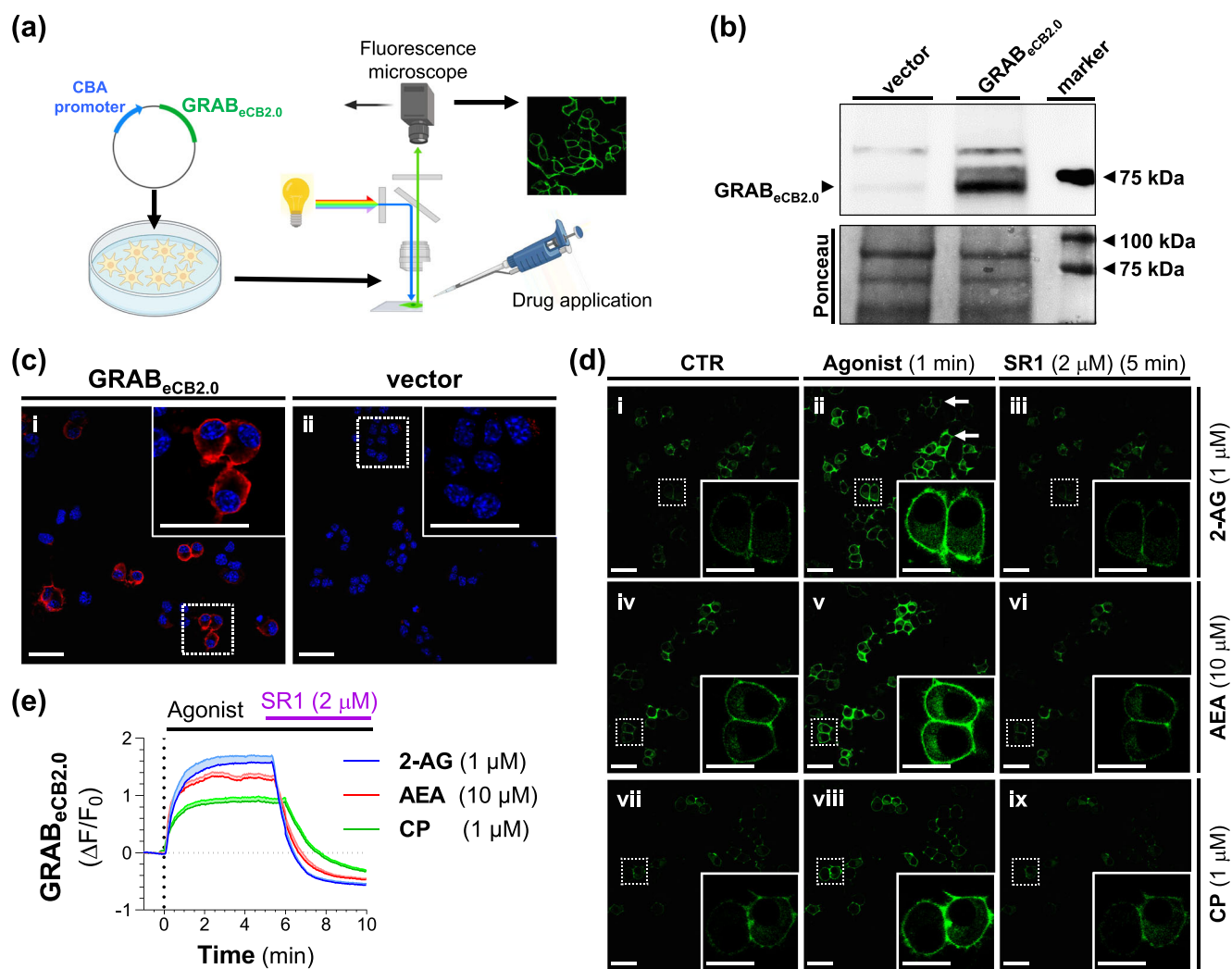


**FIGURE 1** CB<sub>1</sub>R agonists increase GRAB<sub>eCB2.0</sub> fluorescence in N2a cells. (a) Live-cell imaging workflow: N2a cells were transfected with eCB2.0 plasmid, the cells were treated with the CB<sub>1</sub>R ligands by adding agents directly into the buffer, and changes in GRAB<sub>eCB2.0</sub> fluorescence were detected using live-cell confocal microscopy. (b,c) GRAB<sub>eCB2.0</sub> protein expression in N2a cells transfected with eCB2.0 plasmid or vector as detected by a CB<sub>1</sub>R C-terminus antibody using: (b) western blotting and (c) fluorescence microscopy. Scale bars: 20  $\mu$ m. (d) Effects of CB<sub>1</sub>R agonists and of SR1 (2  $\mu$ M) on GRAB<sub>eCB2.0</sub> fluorescence measured using live-cell confocal microscopy. GRAB<sub>eCB2.0</sub> signal during: (i) baseline, (ii) treatment with 2-AG (1  $\mu$ M), (iii) followed by SR1 antagonism, (iv) baseline, (v) treatment with AEA (10  $\mu$ M), (vi) followed by SR1 antagonism, (vii) baseline, (viii) treatment with CP (2  $\mu$ M), (ix) followed by SR1-antagonism. GRAB<sub>eCB2.0</sub> signal were captured for: baseline for 30 s prior to agonist treatment, agonist treatment for 5 min, and SR1 antagonism for 5 min. Heterogeneous levels of GRAB<sub>eCB2.0</sub> fluorescence indicated by arrows. Scale bars = 40  $\mu$ m (inset = 20  $\mu$ m). (e) Time course of CB<sub>1</sub>R agonist-induced increase GRAB<sub>eCB2.0</sub> signal ( $\Delta F/F_0$ ), and antagonism of this response by SR1.  $n = 10$ –15 cells per treatment from a single imaging experiment for each agonist; experiments repeated four times with similar results (see Table 1 for summary results). Shaded area represents SEM.

western blot using an antibody directed against the C-terminus of the CB<sub>1</sub>R. Figure 1c shows that GRAB<sub>eCB2.0</sub> expression detected by the CT-CB<sub>1</sub>R antibody and analysed by microscopy was heterogeneous, as expected from transient transfection, and mostly accumulated at the plasma membrane. To measure real-time changes in GRAB<sub>eCB2.0</sub> fluorescence, we used confocal microscopy (line scanning frequency: 200 Hz, 0.388 FPS) and added pharmacological agents directly to the buffer during imaging (Figure 1a). Figure 1d<sub>i-ii</sub> show that prior to agonist treatment, N2a cells exhibited low, yet detectable, basal fluorescent signal at the plasma membrane, and that 2-AG

(1  $\mu$ M) increased this signal within 60 s. Adding the CB<sub>1</sub>R antagonist, SR141617 (SR1, 2  $\mu$ M) reduced this response (Figure 1d<sub>iii</sub>). Similarly, AEA (10  $\mu$ M) and the CB<sub>1</sub>R agonist CP55940 (CP, 1  $\mu$ M) increased GRAB<sub>eCB2.0</sub> signal at the plasma membrane within 60 s, and these responses were reduced by SR1 (Figure 1d<sub>iv-ix</sub>). Note that the level of GRAB<sub>eCB2.0</sub> fluorescence varies in each N2a cell as expected from a heterologous transfection approach (Figure 1d<sub>ii</sub>, arrowheads). Figure 1e shows the time course of activation and inhibition of these GRAB<sub>eCB2.0</sub> responses and emphasizes three results: (1) 2-AG and CP triggered a twofold faster initial response (slope) and

twofold greater maximal response (peak) compared with AEA; (2) 2-AG and AEA triggered a twofold overall greater response (area under the curve) compared with CP; and (3) Agonist responses were blocked by SR1 treatment with comparable decays ( $t$ ) in their signals (values are in Table 1). These results indicate that GRAB<sub>eCB2.0</sub> expressed in N2a cells are activated by the CB<sub>1</sub>R agonists 2-AG, AEA, and CP, and these responses are antagonized by the CB<sub>1</sub>R antagonist SR1.

### 3.2 | Pharmacological profile and dynamics of changes in GRAB<sub>eCB2.0</sub> fluorescent signal in N2a cells

To characterize the pharmacological profile and dynamics of GRAB<sub>eCB2.0</sub> activation in N2a cells in a more high-throughput manner, we leveraged a 96-well fluorescence plate reader assay (3-Hz scanning frequency) (Singh et al., 2023). Thus, basal GRAB<sub>eCB2.0</sub> fluorescent signal was measured for 1 min, plates were removed from the plate reader, pharmacological agents were added to the media, plates were reinserted in the plate reader within 2 min, and GRAB<sub>eCB2.0</sub> fluorescence was measured for 30 min (Figure 2a). To facilitate data analysis, we developed a MATLAB R2021a algorithm, which averages the fluorescence value measured in each well over time, for multiple experiments and at select timepoints (code available at: <https://github.com/StellaLab/StellaLab.git>). Figure 2b,c shows that 2-AG induced a concentration-dependent increase in GRAB<sub>eCB2.0</sub> signal ( $\Delta F/F_0$ ) and initial GRAB<sub>eCB2.0</sub> activation ( $\Delta\Delta F/F_0$  from time = 0 to 2.3 min) that (1) was detectable at 0 s (when cells were reinserted in the plate reader and first fluorescence signal was measured); (2) reached a peak response within minutes; and (3) plateaued for up to 30 min. Importantly, **glycerol** and **arachidonic acid** (AA), hydrolysis products of 2-AG, did not influence GRAB<sub>eCB2.0</sub> signal (Figure S1a,b). Also, AEA induced concentration-dependent increases in GRAB<sub>eCB2.0</sub> signal and GRAB<sub>eCB2.0</sub> activation with a kinetic profile similar to the 2-AG response (Figure 2d,e).

To calculate the potencies of these fluorescent responses, we analysed GRAB<sub>eCB2.0</sub> signals at the tail end of their activation phase (i.e., average  $\Delta F/F_0$  between 3–4 min). Figure 2f shows that 2-AG and AEA activated GRAB<sub>eCB2.0</sub> with EC<sub>50</sub> values of 81 and 58 nM, respectively, responses that are similar to their potencies at CB<sub>1</sub>R (EC<sub>50</sub> = 96 and 69 nM for 2-AG and AEA, respectively, as measured by adenylyl cyclase inhibition) (Farah et al., 2022; Steffens et al., 2005). CP induced concentration-dependent increases in GRAB<sub>eCB2.0</sub> signal with an EC<sub>50</sub> value of 193 nM, a response that was  $\approx$ 100-fold lower than its reported potency at CB<sub>1</sub>R (EC<sub>50</sub> = 1.27–3.11 nM as measured by adenylyl cyclase inhibition) (Eldeeb et al., 2016; Rinaldi-Carmona et al., 1994) (Figure 2f–h). SR1 reduced the GRAB<sub>eCB2.0</sub> signal below basal with an IC<sub>50</sub> value of 449 nM, which is approximately 100-fold less potent than the reported IC<sub>50</sub> value at CB<sub>1</sub>R (Figure 2i,j) (e.g., 5.6 nM when measuring effect of SR1 on CP-induced inhibition of adenylyl cyclase) (Rinaldi-Carmona et al., 1994). To determine if SR1 reduced the GRAB<sub>eCB2.0</sub> signal below basal due to its inverse agonist activity, we tested the neutral CB<sub>1</sub>R antagonist, AM4113 (Sink et al., 2008). AM4113 also reduced the GRAB<sub>eCB2.0</sub> signal below basal (maximum decrease of  $\Delta F/F_0 = -0.23$  with 10  $\mu$ M) indicating that both SR1 and AM4113 are likely inhibiting GRAB<sub>eCB2.0</sub> activation by basal levels of endogenous eCBs (Figure S2b). Pretreatment of N2a cells with SR1 blocked GRAB<sub>eCB2.0</sub> activation induced by 2-AG, AEA, and CP (Figure 2k). 2-AG, AEA, and CP also failed to elicit increases in fluorescence in N2a cells expressing mutant-GRAB<sub>eCB2.0</sub> (mut-GRAB<sub>eCB2.0</sub>), which contains a phenylalanine to alanine (F177A) mutation in the region within the orthosteric binding pocket (Hua et al., 2017; Shim et al., 2011) (Figure 2k). Importantly, mut-GRAB<sub>eCB2.0</sub> was reliably expressed in N2a cells, confirming the use of this genetic control (Figure S1c). Thus, changes in the GRAB<sub>eCB2.0</sub> signal in N2a cells were reliably measured using a fluorescence plate reader. Furthermore, 2-AG and AEA increased GRAB<sub>eCB2.0</sub> signals with EC<sub>50</sub> values comparable to their potencies at the CB<sub>1</sub>R, and these responses were sensitive to SR1 antagonism.

**TABLE 1** Parameters of GRAB<sub>eCB2.0</sub> activation by agonists and reversal by antagonism. N2a cells in culture were transfected with eCB2.0 plasmid and GRAB<sub>eCB2.0</sub> activated by 2-AG (1  $\mu$ M), anandamide (AEA, 10  $\mu$ M), or CP55940 (CP, 1  $\mu$ M), and subsequently antagonized by SR141617 (SR1, 2  $\mu$ M). Changes in fluorescence ( $\Delta F/F_0$ ) were detected using live-cell confocal microscopy. Data are shown as a mean of  $n = 39$ –70 cells from four independent experiments; error bars represent SEM.

PD parameter	Units	CB1R agonists		
		2-AG	CP	AEA
Initial response: slope	( $\times 10^{-2} \Delta F/F_0/s$ )	<b>3.73</b>	<b>2.30</b>	<b>4.33</b>
	(95% CI)	(3.57–3.89)	(2.16–2.44)	(3.97–4.69)
Time to peak	(min)	<b>4.38</b>	<b>3.74</b>	<b>4.64</b>
Maximal response: peak	( $\Delta F/F_0$ )	<b>1.79</b>	<b>0.90</b>	<b>1.69</b>
	(std. error)	0.074	0.058	0.150
Overall response	(area under the curve)	<b>453</b>	<b>239</b>	<b>434</b>
	(std. error)	12	7	20
Antagonism response: $t$	(s)	<b>62.94</b>	<b>42.18</b>	<b>35.5</b>
	(95% CI)	(57.71–69.08)	(40.21–44.31)	(33.22–38.03)

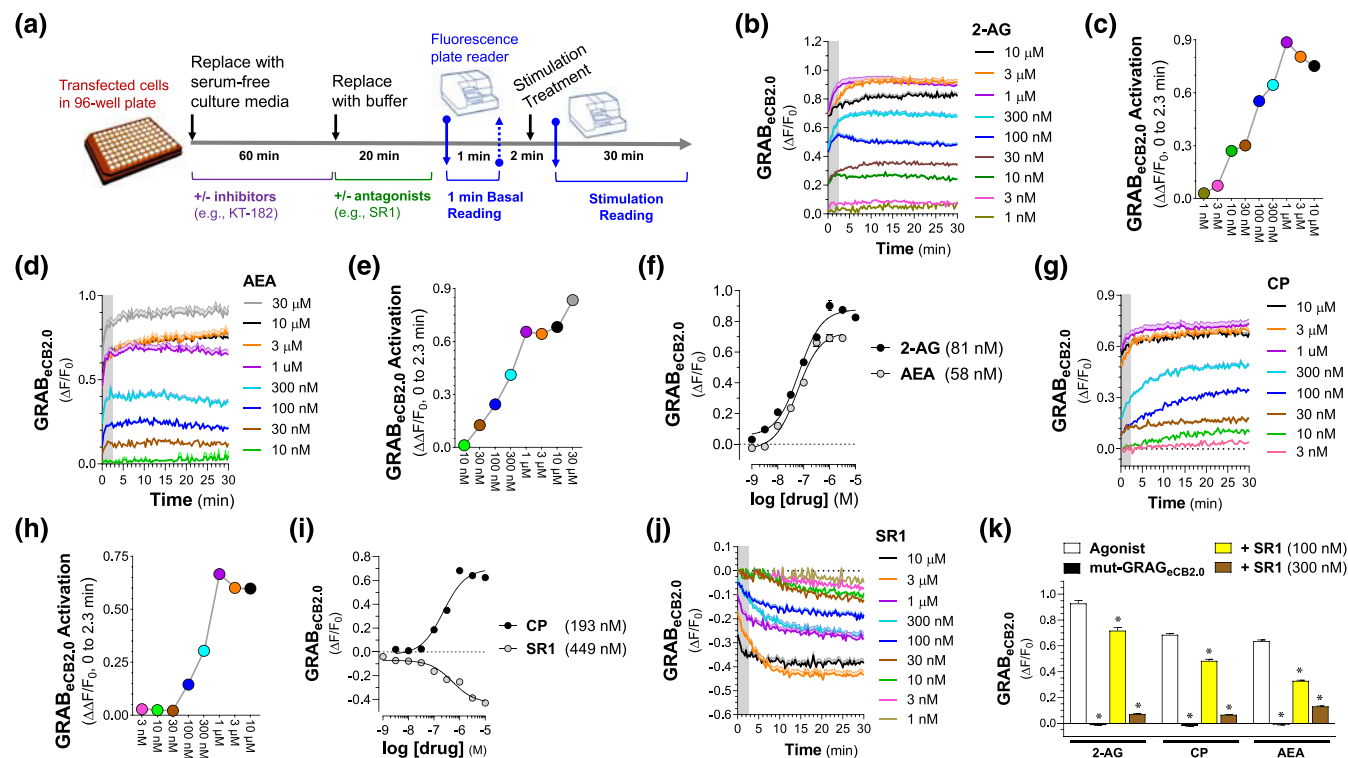


**FIGURE 2** Pharmacological profile of GRAB<sub>eCB2.0</sub> expressed by N2a cells. (a) Workflow for measuring changes in GRAB<sub>eCB2.0</sub> fluorescence using a 96-well plate reader. (b) Time course of the 2-AG concentration-dependent increase in GRAB<sub>eCB2.0</sub> fluorescence ( $\Delta F/F_0$ ) and (c) its activation phase ( $\Delta\Delta F/F_0$  from 0 to 2.3 min). (d) Time course of the AEA concentration-dependent increase in GRAB<sub>eCB2.0</sub> fluorescence and (e) its activation phase ( $\Delta\Delta F/F_0$  from 0 to 2.3 min). (f) Concentration-dependent curves of 2-AG and AEA-induced increases in GRAB<sub>eCB2.0</sub> fluorescence determined by averaging  $\Delta F/F_0$  between 4 and 5 min. (g) Time course of the CP concentration-dependent increase in GRAB<sub>eCB2.0</sub> fluorescence ( $\Delta F/F_0$ ) and (h) its activation phase ( $\Delta\Delta F/F_0$  from 0 to 2.3 min). (i) Concentration–response curves of CP and SR1-induced changes in GRAB<sub>eCB2.0</sub> fluorescent signal as determined by averaging  $\Delta F/F_0$  between 4 and 5 min for CP and from 11–16 min for SR1. (j) Time course of the SR1 concentration-dependent decrease in GRAB<sub>eCB2.0</sub> fluorescence ( $\Delta F/F_0$ ). (k) GRAB<sub>eCB2.0</sub> responses induced by 2-AG (1  $\mu$ M), CP (1  $\mu$ M), and AEA (10  $\mu$ M) in N2a cells either pretreated with SR1 (100 nM and 300 nM) or expressing Mut-GRAB<sub>eCB2.0</sub> as determined by averaging  $\Delta F/F_0$  between 4 and 5 min. Data are shown as mean of  $n = 3$ –76 independent experiments for 2-AG,  $n = 3$ –10 for AEA,  $n = 3$ –39 for CP,  $n = 3$ –5 for 1-AG, and  $n = 4$ –7 for SR1. \* $P < 0.05$  significantly different from corresponding CTR (DMSO 0.1%) treatment (two-way ANOVA followed by Tukey's test). Shaded area in time course and error bars in histograms represent SEM.

### 3.3 | ATP stimulates 2-AG production via P2X<sub>7</sub>R

To determine if ATP stimulates eCB production in N2a cells, we first measured 2-AG and AEA production by LC-MS (see chromatograms, mass spectrums, and detection limits in Figure S3a–k). ATP (300  $\mu$ M) significantly increased 2-AG levels by 53% after 2 min, and this response returned to baseline after 10 min (Figure 3a). By contrast, AEA was below the LC-MS detection limit under both basal and ATP (300  $\mu$ M)-stimulated conditions, indicating that the main eCB produced under these conditions is 2-AG (Figure S3g–i). Figure 3b shows that ATP (300  $\mu$ M) also increased GRAB<sub>eCB2.0</sub> signal as measured by live-cell confocal microscopy. This response increased within seconds of treatment, reaching a maximum  $\Delta F/F_0$  of 0.39 at  $\approx 8$  min. These results indicate that GRAB<sub>eCB2.0</sub> reliably detects endogenous production of 2-AG induced by ATP and that this readout exhibits a more robust and precise dynamic range as compared with LC-MS analysis.

To further characterize the ATP-stimulated increases in 2-AG levels, we measured changes in the GRAB<sub>eCB2.0</sub> signal using the

fluorescence plate reader. Figure 3c shows that ATP induced a concentration-dependent increase in GRAB<sub>eCB2.0</sub> signal with a maximal response reached with 1-mM ATP ( $\Delta F/F_0 = 0.18$  at 10 min). Of note, the 1-mM ATP response was delayed compared with the 300- $\mu$ M ATP response (Figure 3c). We analysed the initial activation rate induced by ATP ( $\Delta\Delta F/F_0$  between 0 min and time at peak response) and the rate of decay ( $\Delta\Delta F/F_0$  between the time at peak response and 30 min). Figure 3d,e shows that ATP induced a concentration-dependent increase in the initial activation of the GRAB<sub>eCB2.0</sub> signal and that the 1-mM ATP response shows a slower decay compared with the 300- $\mu$ M ATP response. Because the GRAB<sub>eCB2.0</sub> detects 2-AG applied at nanomolar concentrations (Figure 2d), we interpolated the increase in endogenous 2-AG concentration induced by ATP (300  $\mu$ M) and estimated an increase in 2-AG levels of  $\approx 9$  nM (Figure S3j).

The high concentration of ATP required to increase 2-AG production suggests the involvement of P2X<sub>7</sub>R (Figure 3f) (Gómez-Villafuertes et al., 2009; Young et al., 2007). Accordingly, the P2X<sub>7</sub>R



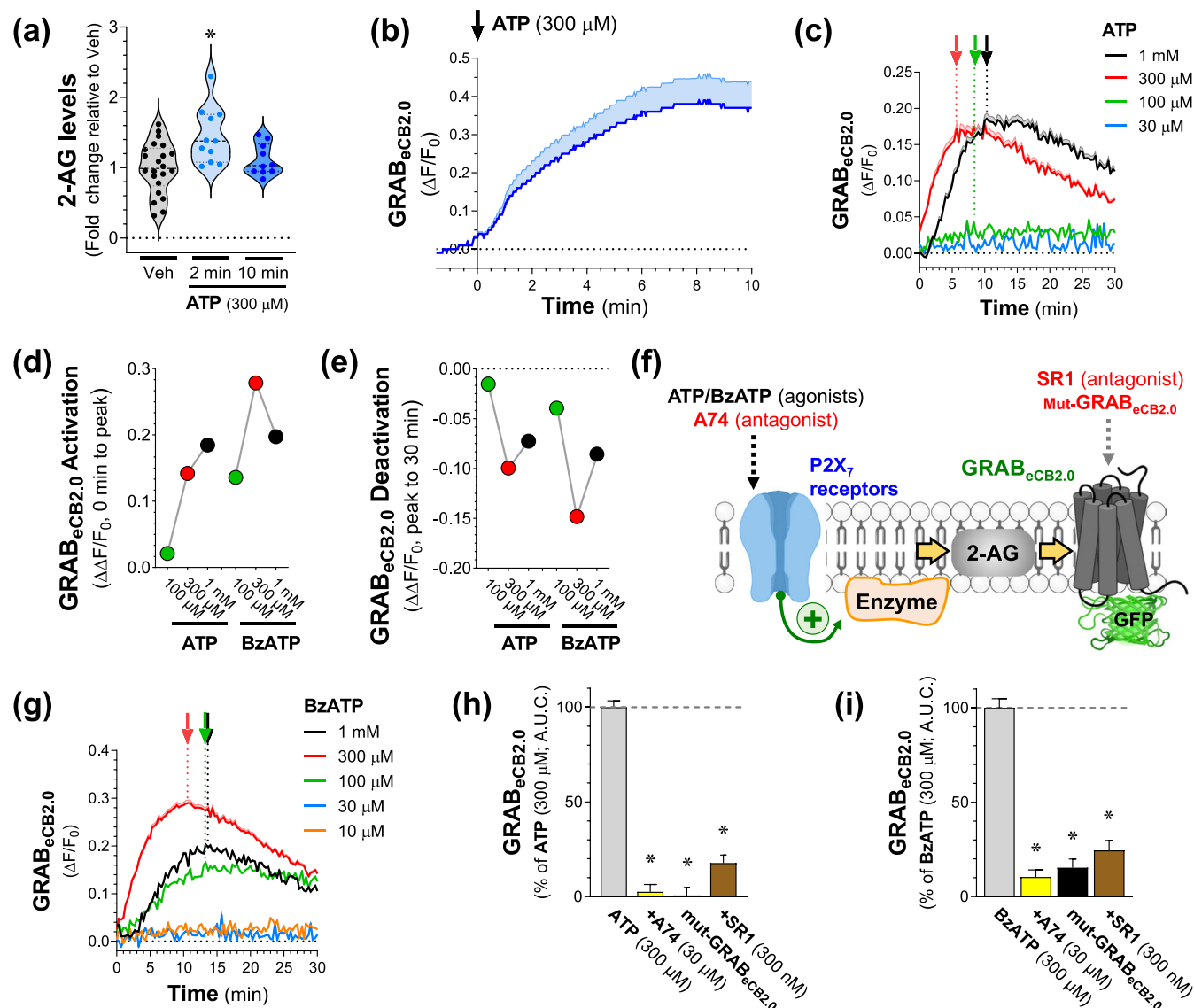


**FIGURE 3** Activation of P2X<sub>7</sub>-R increases 2-AG production by N2a cells. (a) Effect of ATP (300  $\mu$ M for 2 and 10 min) on 2-AG levels in N2a cells as measured by LC-MS/MS. Average 2-AG amounts: 1.07-pmol 2-AG per milligramme of protein for Veh, 1.51-pmol 2-AG per milligramme of protein for 2 min ATP, and 1.25-pmol 2-AG per milligramme of protein for 10 min ATP.  $n = 10$ –22 individual experiments; \* $P < 0.05$  significantly different from vehicle (one-way ANOVA followed by Tukey's test). (b) Effect of ATP (300  $\mu$ M) on GRAB<sub>eCB2.0</sub> fluorescence ( $\Delta F/F_0$ ) measured by live-cell confocal microscopy. Data are shown as a mean of 39 cells from three independent experiments; shaded area represents SEM. (c) Time course of the ATP concentration-dependent increase in GRAB<sub>eCB2.0</sub> fluorescence ( $\Delta F/F_0$ ); detected by fluorescence plate reader. Arrows indicate peak ATP-triggered  $\Delta F/F_0$  responses.  $n = 4$ –23; shaded area of time course signal represents SEM. (d) ATP and BzATP concentration-dependent increase in GRAB<sub>eCB2.0</sub> fluorescence measured during the activation phase ( $\Delta\Delta F/F_0$  from 0 min to peak) and (e) during the deactivation phase ( $\Delta\Delta F/F_0$  from peak to 30 min). (f) Diagram depicting the molecular mechanism of ATP- and BzATP-stimulated 2-AG production and the pharmacological interventions. (g) Time course of the BzATP concentration-dependent increase in GRAB<sub>eCB2.0</sub> fluorescence ( $\Delta F/F_0$ ) as detected by fluorescent plate reader. Arrows indicate peak BzATP-triggered  $\Delta F/F_0$  responses.  $n = 3$ –11. (h,i) Increase in GRAB<sub>eCB2.0</sub> fluorescence induced by ATP (300  $\mu$ M) and BzATP (300  $\mu$ M) in N2a cells either expressing mut-GRAB<sub>eCB2.0</sub>, pretreated with the P2X<sub>7</sub>R antagonist A74003 (A74, 30  $\mu$ M) or pretreated with SR1 (300 nM) as determined by averaging  $\Delta F/F_0$  between 4 and 5 min,  $n = 3$ –8; \* $P < 0.05$  significantly different from corresponding agonist treatment (one-way ANOVA followed by Dunnett's test); error bars represent SEM.

agonist 2'(3')-O-(4-Benzoylbenzoyl)-ATP (BzATP) increased the GRAB<sub>eCB2.0</sub> signal in a concentration-dependent manner (Figure 3g) (Donnelly-Roberts et al., 2009; Janks et al., 2018; Young et al., 2007). The maximum BzATP-induced increase and ensuing decay in GRAB<sub>eCB2.0</sub> response was achieved with 300- $\mu$ M BzATP (maximum  $\Delta F/F_0$

$F_0 = 0.29$  at 11 min), consistent with P2X<sub>7</sub>R involvement, while 1-mM BzATP triggered a delayed initial increase in GRAB<sub>eCB2.0</sub> signal compared with 300- $\mu$ M BzATP (Figure 3d,e,g). Further confirming the involvement of P2X<sub>7</sub>Rs, both 300- $\mu$ M ATP- and BzATP-stimulated responses were blocked by the selective P2X<sub>7</sub>R antagonist, A74003

(30  $\mu\text{M}$ ) without affecting basal  $\text{GRAB}_{\text{eCB2.0}}$  signal (Figure 3h,i and Figure S3<sub>m</sub>) (Donnelly-Roberts et al., 2009; Honore et al., 2006). ATP (300  $\mu\text{M}$ ) and BzATP (300  $\mu\text{M}$ )-induced responses were blocked in N2a cells transfected with mut- $\text{GRAB}_{\text{eCB2.0}}$  and antagonized when pretreated with SR1 (300 nM) (Figure 3h,i). Importantly, treating cells with up to 1 mM of ATP or BzATP for 30 min did not significantly increase lactate dehydrogenase release compared with vehicle, indicating that the changes in the  $\text{GRAB}_{\text{eCB2.0}}$  signal were likely not due to decreased cell viability (Figure S3<sub>n-o</sub>). These results show that ATP-stimulated endogenous 2-AG production from N2a cells involves  $\text{P2X}_7\text{R}$ .

### 3.4 | Calcium- and PLC-dependence of $\text{P2X}_7\text{R}$ -mediated increase in 2-AG production

2-AG production is stimulated by a rise in intracellular calcium that directly activates calcium-sensitive enzymes involved in 2-AG biosynthesis, such as phospholipase C (PLC) (Shonesy et al., 2015; Stella et al., 1997). The  $\text{P2X}_7\text{R}$  is a ligand-gated ion channel and upon activation is permeable to calcium, a response reported in N2a cells (Kopp et al., 2019; Reigada et al., 2017) (Figure 4a). Thus, we hypothesized that activation of the  $\text{P2X}_7\text{R}$  by ATP and BzATP induces 2-AG production by increasing intracellular calcium concentration and that this response involves PLC. Absence of  $[\text{Ca}^{2+}]_e$  in the buffer complemented with the addition of EGTA (1 mM) significantly decreased the ATP (300  $\mu\text{M}$ )- and BzATP (300  $\mu\text{M}$ )-induced increases in  $\text{GRAB}_{\text{eCB2.0}}$  signals, with maximum inhibition of 82% and 67%, respectively, during the activation phase of the response (Figure 4b,c). The BzATP-response was significantly less dependent on  $[\text{Ca}^{2+}]_e$  than the ATP-response, reaching 26% versus 72% during the decay phase of these responses, respectively (Figure 4d). Importantly, the absence of  $\text{Ca}^{2+}_e$  along with EGTA (1 mM) did not affect the basal  $\text{GRAB}_{\text{eCB2.0}}$  signal and direct activation of  $\text{GRAB}_{\text{eCB2.0}}$  by CP (1  $\mu\text{M}$ ), emphasizing the specificity of this treatment (Figure S4a,b). These results show that ATP- and BzATP-stimulated increases in 2-AG levels are differentially dependent on  $[\text{Ca}^{2+}]_e$  influx.

Considering that the absence of  $\text{Ca}^{2+}_e$  resulted in a partial reduction of ATP (300  $\mu\text{M}$ )- and BzATP (300  $\mu\text{M}$ )-induced increases in  $\text{GRAB}_{\text{eCB2.0}}$  signals (Figure 4d), we tested whether mobilization of intracellular calcium contributed to this response. Chelating  $[\text{Ca}^{2+}]_i$  using BAPTA-AM (30  $\mu\text{M}$ ) decreased ATP (300  $\mu\text{M}$ )-stimulated increases in  $\text{GRAB}_{\text{eCB2.0}}$  signals by 38%–61% depending on the phase of the response but only decreased BzATP (300  $\mu\text{M}$ )-stimulated increases in  $\text{GRAB}_{\text{eCB2.0}}$  signals during the activation phase by 37%, indicating that the ATP-stimulated 2-AG production may depend on  $[\text{Ca}^{2+}]_i$  to a greater extent than BzATP-stimulated 2-AG production (Figure 4e–g). Because  $\text{P2X}_7\text{R}$  activation is not thought to trigger  $[\text{Ca}^{2+}]_i$  mobilization from intracellular stores, we tested whether  $\text{P2Y}$  receptor ( $\text{P2YR}$ ) activation and subsequent PLC-dependent intracellular calcium mobilization was involved in these responses (Figure 5a). The  $\text{P2Y}_1\text{R}$  agonist ADP only increased  $\text{GRAB}_{\text{eCB2.0}}$  signal at 1 mM (maximum  $\Delta F/F_0 = 0.15$  at 25.7 min), a concentration known to

activate  $\text{P2X}_7\text{Rs}$  (Figure 5b) (Michel & Fonfria, 2007). However, the  $\text{P2Y}_2\text{R}$  and  $\text{P2Y}_4\text{R}$  agonist UTP induced a concentration-dependent increase in the  $\text{GRAB}_{\text{eCB2.0}}$  signal characterized by peaks (maximum  $\Delta F/F_0 = 0.11$ ) starting at 18 min when cells were treated with 300- $\mu\text{M}$  UTP (Figure 5c). This UTP response was reduced by U73122 (1  $\mu\text{M}$ ), indicating that  $\text{P2Y}_{2/4}\text{R}$  activation increases 2-AG in a PLC-dependent mechanism (Figure 5c) (Burnstock, 2018). Furthermore, the selective  $\text{P2Y}_2\text{R}$  antagonist, AR-C 118925 (AR-C, 1  $\mu\text{M}$ ) reduced the ATP (300  $\mu\text{M}$ )-induced increases in the  $\text{GRAB}_{\text{eCB2.0}}$  signal by 36% only in the decay phase of the response but did not affect the BzATP (300  $\mu\text{M}$ )-induced  $\text{GRAB}_{\text{eCB2.0}}$  signal (Figure 5d–g) (Miras-Portugal et al., 2015). AR-C at 1  $\mu\text{M}$  did not significantly affect the basal  $\text{GRAB}_{\text{eCB2.0}}$  signal but increased the direct activation of  $\text{GRAB}_{\text{eCB2.0}}$  by CP (1  $\mu\text{M}$ ) by 17% (area under the curve), indicating that  $\text{P2Y}_2\text{R}$  antagonism combined with a  $\text{CB}_1\text{R}$  agonist may increase 2-AG production (Figure S4c). To further test the involvement of  $\text{P2Y}_2\text{R}$  in the ATP and BzATP increase 2-AG production, we co-treated N2a cells with BzATP (300  $\mu\text{M}$ ) and UTP (300  $\mu\text{M}$ ) and measured a 72% greater increase in  $\text{GRAB}_{\text{eCB2.0}}$  signal compared with BzATP alone (Figure 5f,g). This response was reduced by  $\approx 68\%$  when N2a cells were pretreated with U73122 (300 nM), confirming the involvement PLC (Figure 5f,g). These results suggest that  $\text{P2Y}_2\text{Rs}$  contribute to ATP-stimulated 2-AG production. Accordingly, the  $\text{P2Y}_2\text{R}$  contributes less than  $\text{P2X}_7\text{Rs}$  ( $\approx 20\%$ ) to the ATP-induced increase in  $\text{GRAB}_{\text{eCB2.0}}$  signal and is dependent on  $[\text{Ca}^{2+}]_i$  mobilization and insensitive to the absence of  $[\text{Ca}^{2+}]_e$ .

Based on this premise, we further studied the involvement of PLC by using U73122, a PLC inhibitor that targets most PLC subtypes. Figure 4e–g shows that U73122 (1  $\mu\text{M}$ ), a concentration known to reduce stimulated 2-AG production in neurons (Stella et al., 1997), decreased the ATP (300  $\mu\text{M}$ )- and BzATP (300  $\mu\text{M}$ )-induced increases in  $\text{GRAB}_{\text{eCB2.0}}$  signal. However, the magnitude of the U73122 effect differed depending on the stimulus (ATP vs. BzATP) and differentially affected the phases of the  $\text{GRAB}_{\text{eCB2.0}}$  response: (1) the ATP-induced activation phase response was inhibited by 58%, whereas the BzATP-induced activation phase response was not affected; (2) the ATP- and BzATP-induced plateau response were inhibited by 45% and 18%, respectively; and (3) in the decay phase, the ATP- and BzATP-induced response were inhibited by 50 and 55%, respectively (Figure 4g). Treatment with U73122 (1  $\mu\text{M}$ ) did not significantly change either the basal  $\text{GRAB}_{\text{eCB2.0}}$  signal or the direct activation of  $\text{GRAB}_{\text{eCB2.0}}$  by CP (1  $\mu\text{M}$ ) within the first 10 min of treatment, although by 30 min of treatment, U73122 decreased CP's signal by 10% (Figure S4c). The delayed increase in the CP-induced  $\text{GRAB}_{\text{eCB2.0}}$  signal may result from an off-target effect, because U73122 can alkylate proteins other than PLC in a time-dependent manner (Leitner et al., 2016). Thus, ATP- and BzATP-stimulated increases in 2-AG production are partially and differentially dependent on PLC activities that are sensitive to U73122: that is, PLC  $\beta 2$  (Hou et al., 2004). We then tested the involvement of phosphoinositide-PLC using its inhibitor, ET-18-OCH<sub>3</sub> (ET-18) (Powis et al., 1992; Sano et al., 2001). Figure 4h,i show that ET-18 (10  $\mu\text{M}$ ), a concentration shown to inhibit 2-AG production in neurons (Stella et al., 1997), also differentially decreased the ATP (300  $\mu\text{M}$ )- and

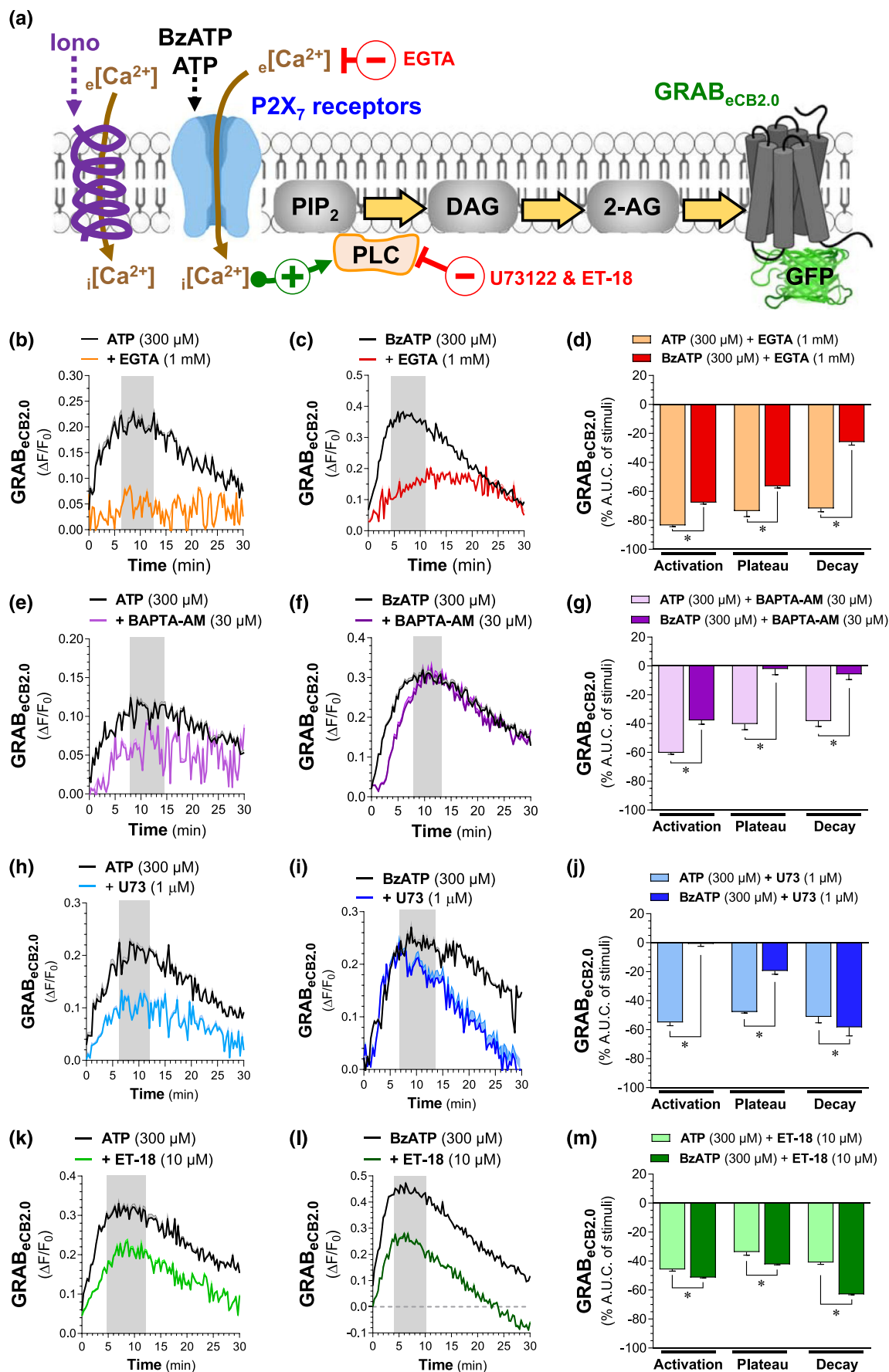
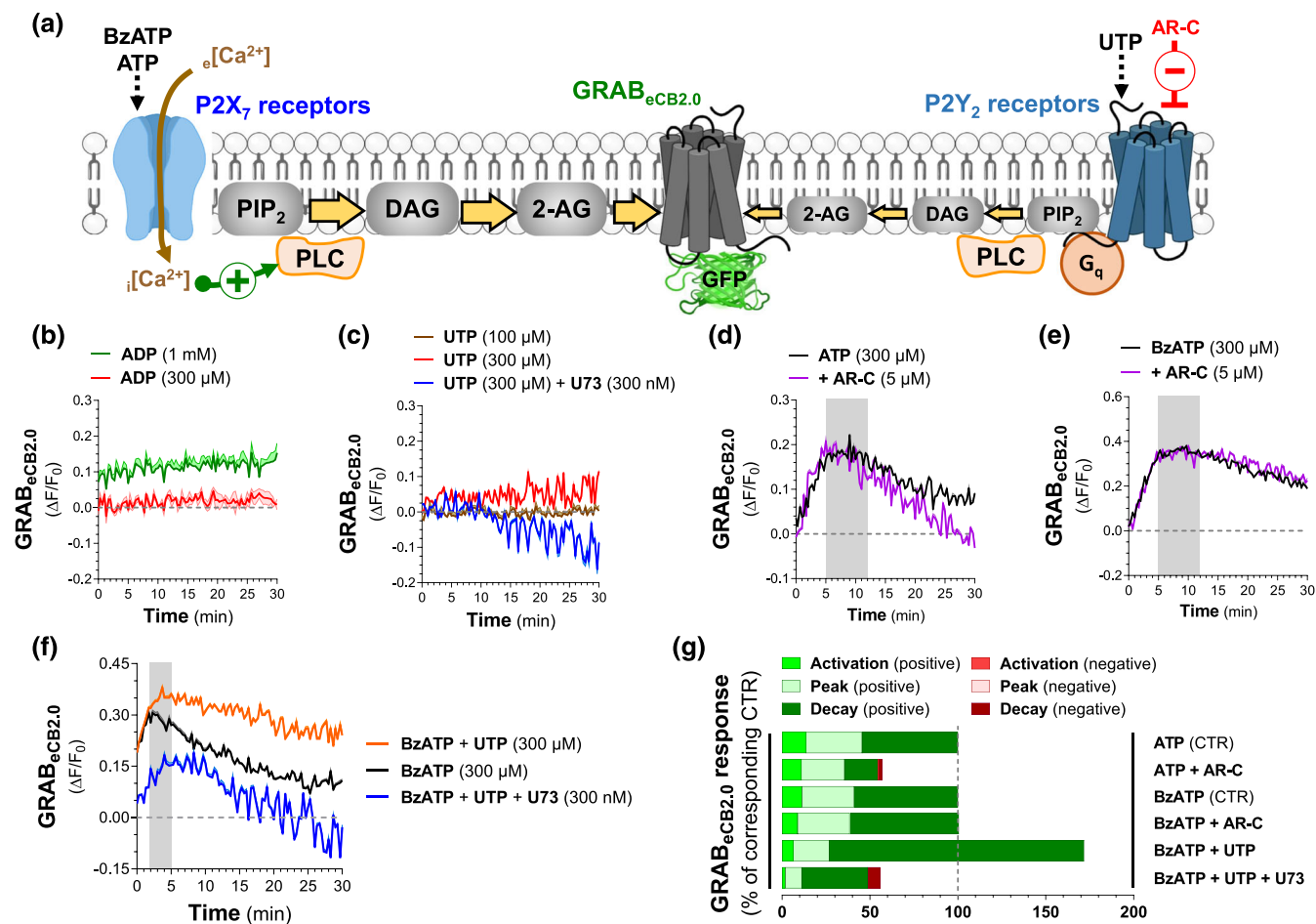


FIGURE 4 Legend on next page.



**FIGURE 5** Role of P2Y<sub>2</sub>R in the ATP-stimulated 2-AG production by N2a. (a) Diagram depicting the involvement of P2Y<sub>2</sub>R in ATP-stimulated 2-AG production and the pharmacological interventions. (b,c) Time courses of changes in GRAB<sub>eCB2.0</sub> fluorescence ( $\Delta F/F_0$ ) following treatment with increasing concentrations of UTP (b), and ADP (c). Effect of U73 (300 nM) on 300- $\mu$ M UTP-stimulated GRAB<sub>eCB2.0</sub> fluorescence. (d,e) Effect of AR-C 118625 (AR-C, 5  $\mu$ M) on GRAB<sub>eCB2.0</sub> fluorescence ( $\Delta F/F_0$ ) stimulated by either 300- $\mu$ M ATP (d) or 300- $\mu$ M BzATP (e). Grey area indicates plateau responses. (f) Effect of UTP (300  $\mu$ M) or combination of UTP (300  $\mu$ M) and U73122 (300 nM) on BzATP (300  $\mu$ M)-stimulated GRAB<sub>eCB2.0</sub> fluorescence ( $\Delta F/F_0$ ). Grey area indicates plateau responses. (g) Quantification of effect of AR-C, UTP, and U73122 on the activation, peak and decay phases of the ATP- and BzATP-stimulated increase in GRAB<sub>eCB2.0</sub> fluorescence ( $\Delta F/F_0$ ) calculated from time courses in (d-f). Results are expressed as % of corresponding CTR (vertical grey dotted line). In (b)–(f),  $n = 3$ –7 independent experiments; shaded area represents SEM.

BzATP (300  $\mu$ M)-induced increases in the GRAB<sub>eCB2.0</sub> signal. This differential inhibition was most significant during the decay phase, where ET-18 inhibited the ATP- and BzATP-induced response by 41% and 63%, respectively (Figure 4j). Treatment with ET-18 (10  $\mu$ M) did not significantly affect the basal GRAB<sub>eCB2.0</sub> signal or direct activation of GRAB<sub>eCB2.0</sub> by CP (1  $\mu$ M) (Figure S4c). These results suggest that P2X<sub>7</sub>R activation stimulates 2-AG production by increasing cytosolic

Ca<sup>2+</sup> and activation of calcium-sensitive PLCs. Accordingly, increasing  $[Ca^{2+}]_i$  with the ionophore ionomycin (2.5  $\mu$ M) was sufficient for increasing 2-AG levels as measured by LC-MS as well as for stimulating an increase in the GRAB<sub>eCB2.0</sub> signal that was PLC-sensitive because it was inhibited by U73122 (300 nM) (Figure S4f–h). Thus, ATP and BzATP stimulate 2-AG production primarily by activating P2X<sub>7</sub>Rs and increasing cytosolic Ca<sup>2+</sup>. This calcium can then activate

**FIGURE 4** P2X<sub>7</sub>R agonists stimulate 2-AG production by N2a cells through an extracellular calcium and PLC dependent mechanism. (a) Diagram depicting the molecular mechanism of P2X<sub>7</sub>R- and ionomycin-dependent increase in 2-AG production and the pharmacological interventions. (b–d) Effect of EGTA (1 mM) and absence of calcium in buffer on the time course of ATP (300  $\mu$ M, b) and BzATP (300  $\mu$ M, c) stimulated increase in GRAB<sub>eCB2.0</sub> fluorescence. Grey area indicates plateau responses. (e–g) Effect of BAPTA-AM (30  $\mu$ M) on the time course of ATP (300  $\mu$ M, e) and BzATP (300  $\mu$ M, f) stimulated increase in GRAB<sub>eCB2.0</sub> fluorescence. (h–j) Effect of U73 (1  $\mu$ M) on the time course of ATP (300  $\mu$ M, h) and BzATP (300  $\mu$ M, i) stimulated increase in GRAB<sub>eCB2.0</sub> fluorescent signal. (k–m) Effect of ET-18-OCH<sub>3</sub> (10  $\mu$ M) on the time course of ATP (300  $\mu$ M, k) and BzATP (300  $\mu$ M, l) stimulated increase in GRAB<sub>eCB2.0</sub> fluorescent signal.  $n = 3$ –6 independent experiments; \* $P < 0.05$  significant difference between ATP and BzATP (two-way ANOVA followed by Šidák's test); shaded areas and error bars represents SEM.

multiple PLCs, including PI-PLC, and the relative contribution of these PLC subtypes is agonist dependent.

### 3.5 | DAGL $\beta$ -dependence and ABHD6-independence of P2X $_7$ R-mediated increase in 2-AG production

DAGL $\beta$  activity is stimulated by calcium, which increases DAG hydrolysis at the *sn*-1 position to generate 2-AG (Eichmann & Lass, 2015). To test the involvement of DAGL in the P2X $_7$ R-dependent increase in 2-AG production, we used its inhibitor DO34 (Figure 6a) (Ogasawara et al., 2016). Because N2a cells have been reported to express DAGL (Jung et al., 2011), we first confirmed DAGL activity in N2a cells and its inhibition by DO34 using activity-based protein profiling (ABPP) (van Esbroeck et al., 2019). Figure 6b shows that N2a cells express robust DAGL $\beta$  activity but no detectable DAGL $\alpha$  activity when compared with mouse cortical membrane proteome (see Figure S6a). DO34 inhibited DAGL $\beta$  with an IC $_{50}$  = 8.1 nM and reduced DAGL $\beta$  activity by 88% at 30 nM (Figure 6c). DO34 (10 nM) fully blocked both the ATP (300  $\mu$ M) and BzATP (300  $\mu$ M)-induced increases in the

GRAB $_{eCB2.0}$  signal (Figure 6d,e,g,h). These results suggest that DAGL $\beta$  mediated the P2X $_7$ R induces increase in 2-AG production by N2a cells. Notably, DO34 treatment followed by either ATP or BzATP decreased GRAB $_{eCB2.0}$  signal below basal, and this decrease was only significant during the decay phase of the response (Figure 6f,i). This effect is likely due to the changes in plasma membrane fluidity following prolonged P2X $_7$ R activation (Drysdale et al., 2022) because DO34 by itself did not affect GRAB $_{eCB2.0}$  signal (Figure S6f,g) (see Section 4).

ABPP analysis also confirmed previous studies showing that N2a cells express ABHD6 activity (Figure 6b) and no MAGL activity (Figure S6b) (Hsu et al., 2013; Marrs et al., 2010; van Esbroeck et al., 2019). We discovered that DO34 also inhibited ABHD6 with an IC $_{50}$  = 8.1 nM, and this response reached 54% at 30 nM (Figure 6c). ABHD6 is a multifunctional enzyme that produces 2-AG from DAG under basal conditions in N2a cells (van Esbroeck et al., 2019) but hydrolyses 2-AG in stimulated neurons (Marrs et al., 2010). To test if ABHD6 controls the P2X $_7$ R-dependent increase in 2-AG production in N2a cells, we used its recently developed inhibitor, AM12100 (Figure 6a) (Kokona et al., 2021; Malamas et al., 2021). ABPP analysis showed that AM12100 inhibited ABHD6 activity with an IC $_{50}$  = 19 nM and reduced ABHD6 activity by 74% at 30 nM without

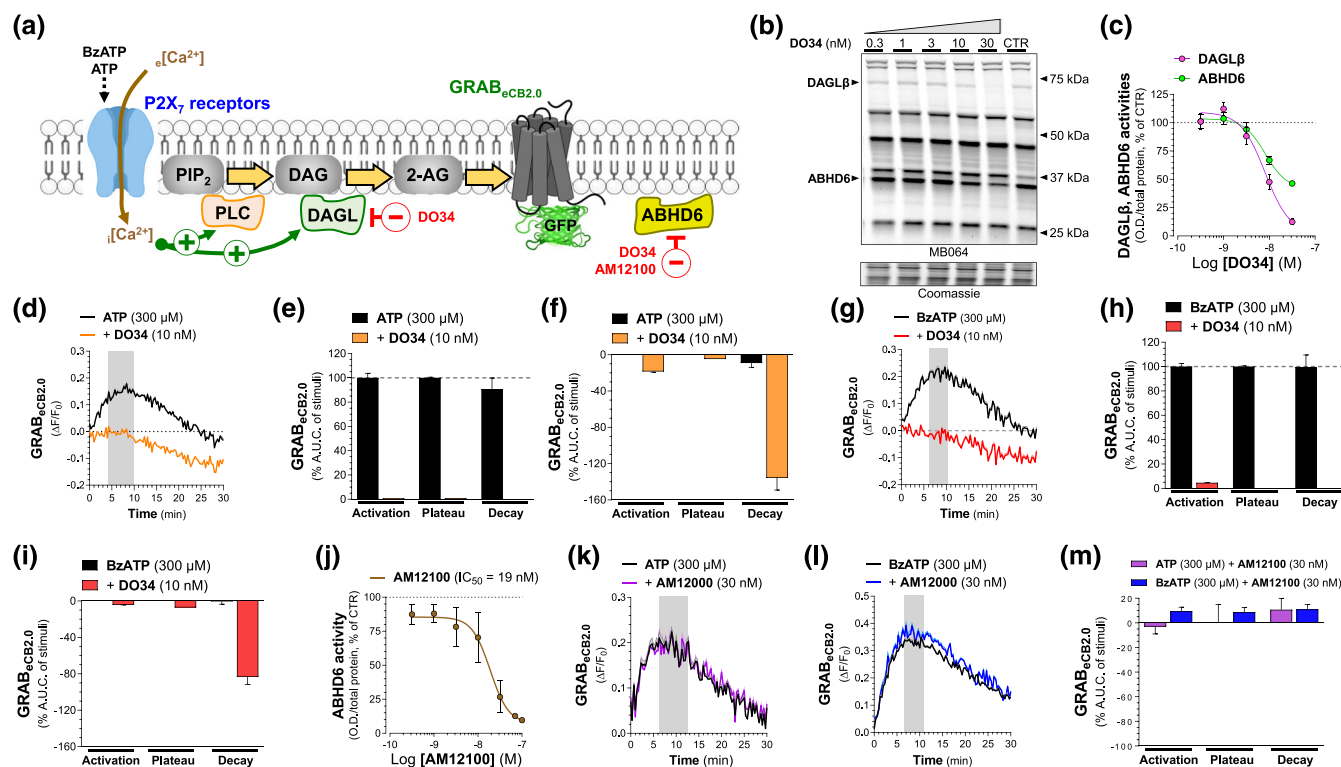


**FIGURE 6** DAGL $\beta$ , but not ABHD6, controls ATP- and BzATP-stimulated 2-AG production by N2a cells. (a) Diagram depicting the involvement of DAGL $\beta$  in P2X $_7$ R dependent increase in 2-AG production and the pharmacological interventions. (b) Concentration-dependent effect of DO34 treatment on activity of endogenously expressed DAGL $\beta$  and ABHD6 in the membrane proteome of N2a cells. Enzyme activity was detected using ABPP with MB064 (2  $\mu$ M, 15 min) as the activity-based probe. (c) Potency of DO34 inhibition of DAGL $\beta$  and ABHD6 activity as quantified by ABPP in (b).  $n = 4-7$  independent experiments. Error bars represent SEM. (d-i) Effect of DO34 (10 nM, 30 min) on the time course of ATP- and BzATP-induced increase in GRAB $_{eCB2.0}$  fluorescence ( $\Delta F/F_0$ ). Area under the curve above 0 (e & h). Area under the curve below 0 (f & i).  $n = 6$  independent experiments. Shaded area represents SEM. (j) Potency of AM12100 inhibition of ABHD6 activity as quantified from ABPP.  $n = 3-5$  independent experiments. Error bars represent SEM. (k-m) Effect of AM12100 (30 nM, 60 min) on the time course of ATP- and BzATP-induced increase in GRAB $_{eCB2.0}$  fluorescence ( $\Delta F/F_0$ ).  $n = 4$  independent experiments. Shaded area represents SEM.

affecting DAGL $\beta$  activity (Figure 6j and Figure S6f,h). Figure 6k-m shows that AM12100 (30 nM) did not significantly affect the ATP (300  $\mu$ M)- and BzATP (300  $\mu$ M)-induced increases in the GRAB<sub>eCB2.0</sub> signal. These results show that P2X<sub>7</sub>R-induced increase in 2-AG production by N2a cells requires DAGL $\beta$  activity but not ABHD6.

## 4 | DISCUSSION

### 4.1 | Pharmacological profile of GRAB<sub>eCB2.0</sub> expressed in N2a cells

We show that 2-AG and AEA increase the GRAB<sub>eCB2.0</sub> signal in N2a cells in seconds and with potencies comparable to their potencies at the CB<sub>1</sub>R; however, CP and SR1 have lower potencies at the GRAB<sub>eCB2.0</sub> compared with their potencies at the CB<sub>1</sub>R (An et al., 2020; Burkey et al., 1997; Eldeeb et al., 2016) (Figure 2). It should be emphasized that these potencies are affected by a multitude of factors, including the model system, receptor expression levels, and assay used to measure receptor activation; therefore, these comparisons only serve to emphasize that the GRAB<sub>eCB2.0</sub> in N2a cells can detect physiologically relevant levels of eCBs. We recently reported the pharmacological profile of GRAB<sub>eCB2.0</sub> sensor expressed by HEK293 cells (Singh et al., 2023) and sought to note several key differences with results gathered in N2a cells: (1) 2-AG increased the GRAB<sub>eCB2.0</sub> signal with similar potencies in both N2a and HEK293 cells while AEA's potency (as EC<sub>50</sub> values) in N2a cells was 58 nM compared with 815 nM in HEK293 cells; this might be due to differential expression of endogenous AEA inactivating enzymes because AEA can be hydrolysed or oxidized by multiple mechanisms (Biringier, 2021). (2) in N2a cells, CP induced a full agonist GRAB<sub>eCB2.0</sub> response (i.e., comparable to 2-AG's response) but a partial agonist GRAB<sub>eCB2.0</sub> response in HEK293 cells. (3) SR1 decreased the GRAB<sub>eCB2.0</sub> signal in N2a cells with an IC<sub>50</sub> value of 449 nM compared with 3.3 nM in HEK293 cells, most likely because of the presence and absence of endogenously expressed CB<sub>1</sub>Rs in these cell lines, respectively (Graham et al., 2006). These results emphasize the need to characterize the GRAB<sub>eCB2.0</sub> pharmacological profile in each model system because it may differ depending on factors, such as GRAB<sub>eCB2.0</sub> expression levels and trafficking as well as the expression profile of eCB hydrolysing enzymes, fatty acid binding proteins, CB<sub>1</sub>Rs, and CB<sub>1</sub>R-interacting proteins (Busquets-Garcia et al., 2018). Importantly, we used undifferentiated N2a cells in this study; thus, the changes in the GRAB<sub>eCB2.0</sub> signal may vary in differentiated N2a cells because expression of the molecular components of eCB signalling changes as they differentiate (van Esbroeck et al., 2019; Wu et al., 2009).

The dynamic range, spatial, and temporal resolution of measuring changes in 2-AG levels in N2a cells detected by GRAB<sub>eCB2.0</sub> is greatly improved compared with LC-MS analysis because it detects real-time 2-AG changes predominantly localized to the plasma membrane within seconds, whereas LC-MS measures total 2-AG content in cells (i.e., plasma membranes and intracellular organelles) at specific time points of sample collection, which limits throughput. Furthermore,

GRAB<sub>eCB2.0</sub> sensor detects nanomolar concentrations of both 2-AG and AEA. LC-MS analysis showed that N2a cells under basal and ATP-stimulated conditions did not produce detectable AEA; thus, AEA is unlikely to contribute to P2X<sub>7</sub>R-mediated increases in GRAB<sub>eCB2.0</sub> signal. This conclusion is further strengthened by P2X<sub>7</sub>R-mediated increases in GRAB<sub>eCB2.0</sub> signal depending on DAGL, which does not produce AEA.

### 4.2 | Calcium- and PLC-dependence of the P2X<sub>7</sub>R mediated increase in 2-AG production

We show that ATP and BzATP increase the GRAB<sub>eCB2.0</sub> signal and that these responses are blocked by the selective P2X<sub>7</sub>R antagonist, A740003. However, ATP and BzATP exhibited remarkable differences in their GRAB<sub>eCB2.0</sub> responses, such as their requirement for [Ca<sup>2+</sup>]<sub>e</sub> during the decay phase of the GRAB<sub>eCB2.0</sub> signal stimulated by ATP compared with BzATP as indicated by a greater inhibition when eliminating [Ca<sup>2+</sup>]<sub>e</sub> (Figure 4b-d). This result may reflect the known differences in the potency and kinetics of P2X<sub>7</sub>R activation by ATP and BzATP: for example, activation of the P2X<sub>7</sub>R by ATP takes several seconds to minutes whereas BzATP is more potent and activates P2X<sub>7</sub>R faster, within a few seconds or less (Kopp et al., 2019). Thus, our study provides an additional example where ATP and BzATP may differentially activate P2X<sub>7</sub>R-dependent signalling pathways, here resulting in differences in 2-AG production (Rassendren et al., 1997).

High micromolar concentrations of ADP, a P2Y<sub>1</sub>R agonist, did not increase the GRAB<sub>eCB2.0</sub> signal, whereas the P2Y<sub>2/4</sub>R agonist UTP induced a small and significant increase in the GRAB<sub>eCB2.0</sub> signal that is sensitive to PLC inhibition, indicating that P2Y<sub>2/4</sub>R activation may contribute to 2-AG production in ATP-treated N2a cells (Erb & Weisman, 2012). Accordingly, (1) absence of [Ca<sup>2+</sup>]<sub>e</sub> partially reduced the ATP and BzATP-stimulated increases in the GRAB<sub>eCB2.0</sub> signal, which suggests P2Y<sub>2</sub>R-dependent mobilization of [Ca<sup>2+</sup>]<sub>i</sub> and (2) BAPTA-AM inhibits both ATP's and BzATP's responses, although with different magnitudes and kinetics (chelating [Ca<sup>2+</sup>]<sub>i</sub> reduced the activation phase of the GRAB<sub>eCB2.0</sub> signal induced by ATP and BzATP and only inhibited the plateau and decay phase of the ATP response). One explanation is that the massive influx of calcium from the extracellular milieu resulting from the P2X<sub>7</sub>R opening is partially chelated by BAPTA and reduces the direct activation of calcium-dependent PLC during the initial phase of the GRAB<sub>eCB2.0</sub> response. Furthermore, the difference in BAPTA's effect on the plateau and decay phase of the ATP response versus the BzATP response suggests a different source of intracellular calcium in the ATP response, possibly via PLC activation and increase in IP<sub>3</sub> and [Ca<sup>2+</sup>]<sub>i</sub> (Kopp et al., 2019). Hence, the selective P2Y<sub>2</sub>R antagonist AR-C118925 significantly inhibited the ATP response without affecting the BzATP response. Together, these results show that while P2X<sub>7</sub>R activation is likely the main mechanism underlying the increased 2-AG production in N2a cells treated with ATP, activation of P2Y<sub>2</sub>R likely contributes to this response. One interpretation is that mechanistic synergism exists between the P2X<sub>7</sub>R and P2Y<sub>2</sub>R activation and that P2Y<sub>2</sub>R activation

alone is not sufficient for stimulating 2-AG production, as suggested by UTP alone having a small effect on the GRAB<sub>eCB2.0</sub> signal but enhancing the BzATP-stimulated GRAB<sub>eCB2.0</sub> signal (Figure 5f).

Few pharmacological tools are available to test the involvement of PLCs and their subtypes. The putative mechanism of action of the aminosteroid, U73122, is the irreversible inhibition of PLC activities through alkylation of cysteines; however, it can also interfere with G protein-dependent activation of PLC and instead deplete plasma membrane phosphoinositol by inhibiting lipid kinases (Horowitz et al., 2005; Thompson et al., 1991). Accordingly, the inhibitory activity of U73122 depends on many factors, including the type of stimuli and model system studied, because it inhibits multiple PLC subtypes and off-targets and also because distinct cell types express different profiles of PLC subtypes. For example, while U73122 inhibits the increased production of 2-AG stimulated by **NMDA ion channels** by neurons in culture but does not inhibit PLC directly activated by calcium (such as those induced by ionomycin in neuronal cells in culture) (Jin et al., 1994). Here, we tested U73122 at concentrations approaching its average reported IC<sub>50</sub> value (i.e., 1 μM) to minimize off-target activity and a chemically distinct inhibitor, ET-18, at concentrations approaching its average reported IC<sub>50</sub> value (i.e., 10 μM) (Horowitz et al., 2005; Powis et al., 1992; Stella et al., 1997). The partial and differential inhibition of the ATP- and BzATP-induced increases in the GRAB<sub>eCB2.0</sub> signal by U73122 and ET-18 suggests (1) multiple PLC subtypes may be involved in P2X<sub>7</sub>R-dependent 2-AG production in N2a cells, (2) distinct PLCs are engaged within seconds, and (3) PLC subtype involvement changes as a function of time. Genetic manipulations and live-cell imaging approaches that facilitate examination of specific PLC enzymes within seconds will be necessary to uncover the precise molecular link between P2X<sub>7</sub>R activation and the specific PLC subtypes that are activated by influx of e[Ca<sup>2+</sup>].

### 4.3 | Testing the involvement of DAGLβ and ABHD6 with DO34 and AM12100

Two isoforms, DAGLα and β, have been characterized, both of which produce 2-AG (Bisogno et al., 2003). Here we confirm that N2a cells only express DAGLβ activity as measured by ABPP (van Esbroeck et al., 2019). Treatment of N2a cells with DO34 (10 nM) inhibited DAGLβ activity by 55% and fully blocked both the ATP- and BzATP-induced increases in the GRAB<sub>eCB2.0</sub> signal, suggesting that DAGLβ represents a rate-limiting step in 2-AG production. It is important to emphasize that knockdown of DAGLβ in N2a cells did not affect 2-AG levels in a previous study (van Esbroeck et al., 2019) and that this finding focused on basal 2-AG levels (i.e., in unstimulated and differentiated N2a cells), whereas here we stimulated 2-AG production in undifferentiated N2a cells. Furthermore, in N2a cells treated with DO34, both the ATP- and BzATP-induced increases in GRAB<sub>eCB2.0</sub> signals were followed by a decay that reached values below baseline GRAB<sub>eCB2.0</sub> signal (Figure 6d–g). A possible mechanism for this decrease in GRAB<sub>eCB2.0</sub> signal below basal includes a time-dependent P2X<sub>7</sub>R-induced change in plasma membrane fluidity, which may be

enhanced when DAGL is inhibited, further affecting plasma membrane fluidity and disrupting GRAB<sub>eCB2.0</sub> activity itself (He et al., 2017; Kanellopoulos & Delarasse, 2019; Wang et al., 2004). Another possibility is that prolonged P2X<sub>7</sub>R activation results in the formation of a nonselective membrane pore permeable to molecules up to 900 Da, which is promoted by phosphatidylglycerol (Karasawa et al., 2017).

We discovered that DO34 also inhibits ABHD6 with the same potency as DAGL, although with a lower efficacy. Thus, we tested the ABHD6 inhibitor AM12100 (Kokona et al., 2021; Malamas et al., 2021) and found no effect on basal or ATP- and BzATP-induced GRAB<sub>eCB2.0</sub> signals, indicating that ABHD6 is not involved in either 2-AG production or hydrolysis in these conditions. The absence of ABHD6 involvement may be due to ABHD6 localization not overlapping with the subcellular compartment that expresses the enzymatic machinery involved in the P2X<sub>7</sub>R-induced increase in 2-AG production.

### 4.4 | Pathological relevance

High ATP concentrations (≥100 nM) are required to activate P2X<sub>7</sub>Rs and are released by damaged or dying cells resulting from chronic neuroinflammation and neuropathic pain (Muñoz et al., 2021; Ren & Illes, 2022). P2X<sub>7</sub>R expression is up-regulated in peripheral nerve tissue samples from patients experiencing neuropathic pain, and P2X<sub>7</sub>R inhibition or knock-down demonstrates therapeutic efficacy in pre-clinical models of neuropathic pain and spinal cord injury (Chessell et al., 2005; Ren & Illes, 2022; Wang et al., 2004). Pharmacological enhancement of 2-AG-CB<sub>1</sub>R signalling, for example, with CB<sub>1</sub>R positive allosteric modulators, produce analgesia in rodent pain models (Slivicki et al., 2020). Our study provides further evidence for a mechanistic link between P2X<sub>7</sub>R activation and neuronal 2-AG production, which helps further understand the signalling processes involved in chronic neuroinflammation and neuropathic pain.

### 4.5 | Conclusions

Activation of P2X<sub>7</sub>R expressed by N2a cells in culture increases 2-AG production within seconds, and this response is potentiated by P2Y<sub>2</sub>R following several minutes of agonist exposure. This mechanism depends on [Ca<sup>2+</sup>]<sub>e</sub>, [Ca<sup>2+</sup>]<sub>i</sub>, several PLC subtypes, and DAGLβ and is not controlled by ABHD6, suggesting subcellular compartmentalization of molecular machinery. Thus, our study outlines the molecular mechanism that links increase in [ATP]<sub>e</sub> and enhanced 2-AG production that is involved in chronic neuroinflammation and neuropathic pain.

### AUTHOR CONTRIBUTIONS

S. Singh and D. Sarroza performed 96-well fluorescent imaging. S. Singh performed cloning, live-cell confocal microscopy, and activity-based protein profiling. S. Singh, D. Sarroza, and D. Whittington performed LC-MS/MS. A. English performed MATLAB analysis. S. Singh

and N. Stella designed experiments, analysed data, and wrote the manuscript. B.B. Land, M.R. Bruchas, L. Zweifel, M. van der Stelt, Y. Li, and A. Dong contributed to data interpretation and provided feedback on the manuscript. N. Stella supervised and coordinated research as well as secured funding for the study.

## ACKNOWLEDGEMENTS

This work was supported by the National Institutes of Health (NS118130 and DA047626 to N.S., DA055448 to AE, DA033396 to MRB, and T32GM007750). We would like to acknowledge support from the University of Washington Center of Excellence in Opioid Addiction Research/Molecular Genetics Resource Core (P30DA048736). National Natural Science Foundation of China (31925017 and 31871087), the Beijing Municipal Science & Technology Commission (Z181100001318002 and Z181100001518004), the NIH BRAIN Initiative (1U01NS113358), the Shenzhen-Hong Kong Institute of Brain Science (NYKFKT2019013), the Science Fund for Creative Research Groups of the National Natural Science Foundation of China (81821092) and grants from the Peking-Tsinghua Center for Life Sciences and the State Key Laboratory of Membrane Biology at Peking University School of Life Sciences (to YL).

## CONFLICT OF INTEREST STATEMENT

N.S. is employed by the University of Washington, Seattle, and by Stella Consulting LLC. The terms of this arrangement have been reviewed and approved by the University of Washington in accordance with its policies governing outside work and financial conflicts of interest in research. M.R.B. is a co-founder and SAB member of NeuroLux, Inc. None of the technology or work described here is related to those efforts. All other authors declare that they do not have any known competing financial interests or relationships that could have influenced the work in this paper.

## DATA AVAILABILITY STATEMENT

The data that support the findings of this study are available from the corresponding author upon reasonable request.

## DECLARATION OF TRANSPARENCY AND SCIENTIFIC RIGOUR

This Declaration acknowledges that this paper adheres to the principles for transparent reporting and scientific rigour of preclinical research as stated in the *BJP* guidelines for [Natural Products Research, Design and Analysis](#), and [Immunoblotting and Immunochemistry](#), and as recommended by funding agencies, publishers and other organizations engaged with supporting research.

## ORCID

Simar Singh  <https://orcid.org/0000-0001-5785-8292>

## REFERENCES

- Alexander, S. P. H., Christopoulos, A., Davenport, A. P., Kelly, E., Mathie, A. A., Peters, J. A., Veale, E. L., Armstrong, J. F., Faccenda, E., Harding, S. D., Davies, J. A., Abbracchio, M. P., Abraham, G.,

Agoulnik, A., Alexander, W., Al-Hosaini, K., Bäck, M., Baker, J. G., Barnes, N. M., ... Ye, R. D. (2023). The concise guide to PHARMACOLOGY 2023/24: G protein-coupled receptors. *British Journal of Pharmacology*, 180, S23–S144.

Alexander, S. P. H., Fabbro, D., Kelly, E., Mathie, A. A., Peters, J. A., Veale, E. L., Armstrong, J. F., Faccenda, E., Harding, S. D., Davies, J. A., Annett, S., Boison, D., Burns, K. E., Dessauer, C., Gertsch, J., Helsby, N. A., Izzo, A. A., Ostrom, R., Papapetropoulos, A., ... Wong, S. S. (2023). The concise guide to PHARMACOLOGY 2023/24: Enzymes. *British Journal of Pharmacology*, 180, S289–S373. <https://doi.org/10.1111/bph.16179>

Alexander, S. P. H., Mathie, A. A., Peters, J. A., Veale, E. L., Striessnig, J., Kelly, E., Armstrong, J. F., Faccenda, E., Harding, S. D., Davies, J. A., Aldrich, R. W., Attali, B., Baggetta, A. M., Becirovic, E., Biel, M., Bill, R. M., Caceres, A. I., Catterall, W. A., Conner, A. C., ... Zhu, M. (2023). The concise guide to PHARMACOLOGY 2023/24: Ion channels. *British Journal of Pharmacology*, 180, S145–S222.

An, D., Peigneur, S., Hendrickx, L. A., & Tytgat, J. (2020). Targeting cannabinoid receptors: Current status and prospects of natural products. *International Journal of Molecular Sciences*, 21, 5064. <https://doi.org/10.3390/ijms21145064>

Andrejew, R., Oliveira-Giacomelli, Á., Ribeiro, D. E., Glaser, T., Arnaud-Sampaio, V. F., Lameu, C., & Ulrich, H. (2020). The P2X7 receptor: Central hub of brain diseases. *Frontiers in Molecular Neuroscience*, 13, 124. <https://doi.org/10.3389/fnmol.2020.00124>

Baggelaar, M. P., Chameau, P. J. P., Kantae, V., Hummel, J., Hsu, K.-L., Janssen, F., van der Wel, T., Soethoudt, M., Deng, H., den Dulk, H., Allarà, M., Florea, B. I., di Marzo, V., Wadman, W. J., Kruse, C. G., Overkleeft, H. S., Hankemeier, T., Werkman, T. R., Cravatt, B. F., & van der Stelt, M. (2015). Highly selective, reversible inhibitor identified by comparative chemoproteomics modulates diacylglycerol lipase activity in neurons. *Journal of the American Chemical Society*, 137, 8851–8857. <https://doi.org/10.1021/jacs.5b04883>

Baggelaar, M. P., Maccarrone, M., & van der Stelt, M. (2018). 2-Arachidonylglycerol: A signaling lipid with manifold actions in the brain. *Progress in Lipid Research*, 71, 1–17. <https://doi.org/10.1016/j.plipres.2018.05.002>

Biringer, R. G. (2021). The rise and fall of anandamide: Processes that control synthesis, degradation, and storage. *Molecular and Cellular Biochemistry*, 476, 2753–2775. <https://doi.org/10.1007/s11010-021-04121-5>

Bisogno, T., Howell, F., Williams, G., Minassi, A., Cascio, M. G., Ligresti, A., Matias, I., Schiano-Moriello, A., Paul, P., Williams, E. J., Gangadharan, U., Hobbs, C., di Marzo, V., & Doherty, P. (2003). Cloning of the first sn1-DAG lipases points to the spatial and temporal regulation of endocannabinoid signaling in the brain. *The Journal of Cell Biology*, 163, 463–468. <https://doi.org/10.1083/jcb.200305129>

Burkey, T. H., Quock, R. M., Consroe, P., Ehlert, F. J., Hosohata, Y., Roeske, W. R., & Yamamura, H. I. (1997). Relative efficacies of cannabinoid CB1 receptor agonists in the mouse brain. *European Journal of Pharmacology*, 336, 295–298. [https://doi.org/10.1016/S0014-2999\(97\)01255-7](https://doi.org/10.1016/S0014-2999(97)01255-7)

Burnstock, G. (2018). Purine and purinergic receptors. *Brain and Neuroscience Advances*, 2, 2398212818817494.

Busquets-García, A., Bains, J., & Marsicano, G. (2018). CB(1) receptor signaling in the brain: Extracting specificity from ubiquity. *Neuropsychopharmacology*, 43, 4–20. <https://doi.org/10.1038/npp.2017.206>

Chavez-Noriega, L. E., Crona, J. H., Washburn, M. S., Urrutia, A., Elliott, K. J., & Johnson, E. C. (1997). Pharmacological characterization of recombinant human neuronal nicotinic acetylcholine receptors  $\alpha 2\beta 2$ ,  $\alpha 2\beta 4$ ,  $\alpha 3\beta 2$ ,  $\alpha 3\beta 4$ ,  $\alpha 4\beta 2$ ,  $\alpha 4\beta 4$  and  $\alpha 7$  expressed in *Xenopus* oocytes. *Journal of Pharmacology and Experimental Therapeutics*, 280, 346–356.

Chessell, I. P., Hatcher, J. P., Bountra, C., Michel, A. D., Hughes, J. P., Green, P., Egerton, J., Murfin, M., Richardson, J., Peck, W. L.,



- Grahames, C. B. A., Casula, M. A., Yiangou, Y., Birch, R., Anand, P., & Buell, G. N. (2005). Disruption of the P2X7 purinoceptor gene abolishes chronic inflammatory and neuropathic pain. *Pain*, 114, 386–396. <https://doi.org/10.1016/j.pain.2005.01.002>
- Covelo, A., Eraso-Pichot, A., Fernández-Moncada, I., Serrat, R., & Marsicano, G. (2021). CB1R-dependent regulation of astrocyte physiology and astrocyte-neuron interactions. *Neuropharmacology*, 195, 108678. <https://doi.org/10.1016/j.neuropharm.2021.108678>
- Curtis, M. J., Alexander, S. P. H., Cirino, G., George, C. H., Kendall, D. A., Insel, P. A., Izzo, A. A., Ji, Y., Panettieri, R. A., Patel, H. H., Sobey, C. G., Stanford, S. C., Stanley, P., Stefanska, B., Stephens, G., Teixeira, M. M., Vergnolle, N., & Ahluwalia, A. (2022). Planning experiments: Updated guidance on experimental design and analysis and their reporting III. *British Journal of Pharmacology*, 179(15), 3907–3913. <https://doi.org/10.1111/bph.15868>
- Dong, A., He, K., Dudok, B., Farrell, J. S., Guan, W., Liput, D. J., Puhl, H. L., Cai, R., Wang, H., Duan, J., Albarran, E., Ding, J., Lovinger, D. M., Li, B., Soltesz, I., & Li, Y. (2021). A fluorescent sensor for spatiotemporally resolved imaging of endocannabinoid dynamics in vivo. *Nature Biotechnology*, 40(5), 787–798.
- Donnelly-Roberts, D. L., Namovic, M. T., Han, P., & Jarvis, M. F. (2009). Mammalian P2X7 receptor pharmacology: Comparison of recombinant mouse, rat and human P2X7 receptors. *British Journal of Pharmacology*, 157, 1203–1214. <https://doi.org/10.1111/j.1476-5381.2009.00233.x>
- Drysdale, C., Park, K., Vessey, K. A., Huang, X., Caruso, E., Li, Y., Wong, J., Wiley, J. S., Fletcher, E., Guymer, R. H., & Gu, B. J. (2022). P2X7-mediated alteration of membrane fluidity is associated with the late stages of age-related macular degeneration. *Purinergic Signal*, 18, 469–479. <https://doi.org/10.1007/s11302-022-09894-y>
- Eichmann, T. O., & Lass, A. (2015). DAG tales: The multiple faces of diacylglycerol—Stereochemistry, metabolism, and signaling. *Cellular and Molecular Life Sciences*, 72, 3931–3952. <https://doi.org/10.1007/s00018-015-1982-3>
- Eldeeb, K., Leone-Kabler, S., & Howlett, A. C. (2016). CB1 cannabinoid receptor-mediated increases in cyclic AMP accumulation are correlated with reduced Gi/o function. *Journal of Basic and Clinical Physiology and Pharmacology*, 27, 311–322. <https://doi.org/10.1515/jbcpp-2015-0096>
- Erb, L., & Weisman, G. A. (2012). Coupling of P2Y receptors to G proteins and other signaling pathways. *Wiley Interdisciplinary Reviews: Membrane Transport and Signaling*, 1, 789–803. <https://doi.org/10.1002/wmts.62>
- van Esbroeck, A. C. M., Kantae, V., di, X., van der Wel, T., den Dulk, H., Stevens, A. F., Singh, S., Bakker, A. T., Florea, B. I., Stella, N., Overkleeft, H. S., Hankemeier, T., & van der Stelt, M. (2019). Identification of  $\alpha,\beta$ -hydrolase domain containing protein 6 as a diacylglycerol lipase in neuro-2a cells. *Frontiers in Molecular Neuroscience*, 12, 286–286. <https://doi.org/10.3389/fnmol.2019.00286>
- Farah, S. I., Hilston, S., Tran, N., Zvonok, N., & Makriyannis, A. (2022). 1-, 2- and 3-AG as substrates of the endocannabinoid enzymes and endogenous ligands of the cannabinoid receptor 1. *Biochemical and Biophysical Research Communications*, 591, 31–36. <https://doi.org/10.1016/j.bbrc.2021.12.105>
- Farrell, J. S., Colangeli, R., Dong, A., George, A. G., Addo-Osafo, K., Kingsley, P. J., Morena, M., Wolff, M. D., Dudok, B., He, K., Patrick, T. A., Sharkey, K. A., Patel, S., Marnett, L. J., Hill, M. N., Li, Y., Teskey, G. C., & Soltesz, I. (2021). In vivo endocannabinoid dynamics at the timescale of physiological and pathological neural activity. *Neuron*, 109, 2398–2403. <https://doi.org/10.1016/j.neuron.2021.05.026>
- Gómez-Villafuertes, R., del Puerto, A., Díaz-Hernández, M., Bustillo, D., Díaz-Hernández, J. I., Huerta, P. G., Artalejo, A. R., Garrido, J. J., & Miras-Portugal, M. T. (2009).  $Ca^{2+}$ /calmodulin-dependent kinase II signalling cascade mediates P2X7 receptor-dependent inhibition of neurogenesis in neuroblastoma cells. *The FEBS Journal*, 276, 5307–5325. <https://doi.org/10.1111/j.1742-4658.2009.07228.x>
- Graham, E. S., Ball, N., Scotter, E. L., Narayan, P., Dragunow, M., & Glass, M. (2006). Induction of Krox-24 by endogenous cannabinoid type 1 receptors in Neuro2A cells is mediated by the MEK-ERK MAPK pathway and is suppressed by the phosphatidylinositol 3-kinase pathway\*. *Journal of Biological Chemistry*, 281, 29085–29095. <https://doi.org/10.1074/jbc.M602516200>
- Grygorczyk, R., Boudreault, F., Ponomarchuk, O., Tan, J. J., Furuya, K., Goldgewicht, J., Kenfack, F., & Yu, F. (2021). Lytic release of cellular ATP: Physiological relevance and therapeutic applications. *Life (Basel)*, 11, 700. <https://doi.org/10.3390/life11070700>
- He, Y., Taylor, N., Fourgeaud, L., & Bhattacharya, A. (2017). The role of microglial P2X7: Modulation of cell death and cytokine release. *Journal of Neuroinflammation*, 14, 135. <https://doi.org/10.1186/s12974-017-0904-8>
- Honore, P., Donnelly-Roberts, D., Namovic, M. T., Hsieh, G., Zhu, C. Z., Mikusa, J. P., Hernandez, G., Zhong, C., Gauvin, D. M., Chandran, P., Harris, R., Medrano, A. P., Carroll, W., Marsh, K., Sullivan, J. P., Faltynek, C. R., & Jarvis, M. F. (2006). A-740003 [N-(1-[[[cyanoimino] (5-quinolinylamino) methyl] amino]-2, 2-dimethylpropyl)-2-(3, 4-dimethoxyphenyl) acetamide], a novel and selective P2X7 receptor antagonist, dose-dependently reduces neuropathic pain in the rat. *Journal of Pharmacology and Experimental Therapeutics*, 319, 1376–1385. <https://doi.org/10.1124/jpet.106.111559>
- Horowitz, L. F., Hirdes, W., Suh, B. C., Hilgemann, D. W., Mackie, K., & Hille, B. (2005). Phospholipase C in living cells: Activation, inhibition,  $Ca^{2+}$  requirement, and regulation of M current. *The Journal of General Physiology*, 126, 243–262. <https://doi.org/10.1085/jgp.200509309>
- Hossain, M. Z., Ando, H., Unno, S., & Kitagawa, J. (2020). Targeting peripherally restricted cannabinoid receptor 1, cannabinoid receptor 2, and endocannabinoid-degrading enzymes for the treatment of neuropathic pain including neuropathic orofacial pain. *International Journal of Molecular Sciences*, 21, 1423. <https://doi.org/10.3390/ijms21041423>
- Hou, C., Kirchner, T., Singer, M., Matheis, M., Argentieri, D., & Cavender, D. (2004). In vivo activity of a phospholipase C inhibitor, 1-(6-((17 $\beta$ -3-methoxyestra-1,3,5(10)-trien-17-yl)amino)hexyl)-1H-pyrrole-2,5-dione (U73122), in acute and chronic inflammatory reactions. *The Journal of Pharmacology and Experimental Therapeutics*, 309, 697–704. <https://doi.org/10.1124/jpet.103.060574>
- Hsu, K.-L., Tsuboi, K., Adibekian, A., Pugh, H., Masuda, K., & Cravatt, B. F. (2012). DAGL $\beta$  inhibition perturbs a lipid network involved in macrophage inflammatory responses. *Nature Chemical Biology*, 8, 999–1007. <https://doi.org/10.1038/nchembio.1105>
- Hsu, K.-L., Tsuboi, K., Chang, J. W., Whitby, L. R., Speers, A. E., Pugh, H., & Cravatt, B. F. (2013). Discovery and optimization of piperidyl-1-, 2,3-triazole ureas as potent, selective, and in vivo-active inhibitors of  $\alpha/\beta$ -hydrolase domain containing 6 (ABHD6). *Journal of Medicinal Chemistry*, 56, 8270–8279. <https://doi.org/10.1021/jm400899c>
- Hua, T., Vemuri, K., Nikas, S. P., Laprairie, R. B., Wu, Y., Qu, L., Pu, M., Korde, A., Jiang, S., Ho, J. H., Han, G. W., Ding, K., Li, X., Liu, H., Hanson, M. A., Zhao, S., Bohn, L. M., Makriyannis, A., Stevens, R. C., & Liu, Z. J. (2017). Crystal structures of agonist-bound human cannabinoid receptor CB(1). *Nature*, 547, 468–471. <https://doi.org/10.1038/nature23272>
- Janks, L., Sharma, C. V. R., & Egan, T. M. (2018). A central role for P2X7 receptors in human microglia. *Journal of Neuroinflammation*, 15, 325. <https://doi.org/10.1186/s12974-018-1353-8>
- Jin, W., Lo, T.-M., Loh, H. H., & Thayer, S. A. (1994). U73122 inhibits phospholipase C-dependent calcium mobilization in neuronal cells. *Brain Research*, 642, 237–243. [https://doi.org/10.1016/0006-8993\(94\)90927-X](https://doi.org/10.1016/0006-8993(94)90927-X)
- Jung, K.-M., Astarita, G., Thongkham, D., & Piomelli, D. (2011). Diacylglycerol lipase- $\alpha$  and - $\beta$  control neurite outgrowth in neuro-2a cells through distinct molecular mechanisms. *Molecular Pharmacology*, 80, 60–67. <https://doi.org/10.1124/mol.110.070458>

- Kanellopoulos, J. M., & Delarasse, C. (2019). Pleiotropic roles of P2X7 in the central nervous system. *Frontiers in Cellular Neuroscience*, 13, 401. <https://doi.org/10.3389/fncel.2019.00401>
- Karasawa, A., Michalski, K., Mikhelzon, P., & Kawate, T. (2017). The P2X7 receptor forms a dye-permeable pore independent of its intracellular domain but dependent on membrane lipid composition. *eLife*, 6, e31186. <https://doi.org/10.7554/eLife.31186>
- Kennedy, C. (2021). The P2Y/P2X divide: How it began. *Biochemical Pharmacology*, 187, 114408. <https://doi.org/10.1016/j.bcp.2021.114408>
- Kokona, D., Spyridakos, D., Tzatzarakis, M., Papadogkonaki, S., Filidou, E., Arvanitidis, K. I., Kolios, G., Lamani, M., Makriyannis, A., Malamas, M. S., & Thermos, K. (2021). The endocannabinoid 2-arachidonoylglycerol and dual ABHD6/MAGL enzyme inhibitors display neuroprotective and anti-inflammatory actions in the in vivo retinal model of AMPA excitotoxicity. *Neuropharmacology*, 185, 108450. <https://doi.org/10.1016/j.neuropharm.2021.108450>
- Kopp, R., Krautloher, A., Ramirez-Fernández, A., & Nicke, A. (2019). P2X7 interactions and signaling—Making head or tail of it. *Frontiers in Molecular Neuroscience*, 12, 183. <https://doi.org/10.3389/fnmol.2019.00183>
- Labouesse, M. A., & Patriarchi, T. (2021). A versatile GPCR toolkit to track in vivo neuromodulation: Not a one-size-fits-all sensor. *Neuropsychopharmacology*, 46, 2043–2047. <https://doi.org/10.1038/s41386-021-00982-y>
- Leitner, M. G., Michel, N., Behrendt, M., Dierich, M., Dembla, S., Wilke, B. U., Konrad, M., Lindner, M., Oberwinkler, J., & Oliver, D. (2016). Direct modulation of TRPM4 and TRPM3 channels by the phospholipase C inhibitor U73122. *British Journal of Pharmacology*, 173, 2555–2569. <https://doi.org/10.1111/bph.13538>
- Lilley, E., Stanford, S. C., Kendall, D. E., Alexander, S. P., Cirino, G., Docherty, J. R., George, C. H., Insel, P. A., Izzo, A. A., Ji, Y., Panettieri, R. A., Sobey, C. G., Stefanska, B., Stephens, G., Teixeira, M., & Ahluwalia, A. (2020). ARRIVE 2.0 and the British Journal of Pharmacology: Updated guidance for 2020. *British Journal of Pharmacology*, 177(16), 3611. <https://doi.org/10.1111/bph.15178>
- Liput, D. J., Puhl, H. L., Dong, A., He, K., Li, Y., & Lovinger, D. M. (2022). 2-Arachidonoylglycerol mobilization following brief synaptic stimulation in the dorsal lateral striatum requires glutamatergic and cholinergic neurotransmission. *Neuropharmacology*, 205, 108916. <https://doi.org/10.1016/j.neuropharm.2021.108916>
- Liu, Z., Yang, N., Dong, J., Tian, W., Chang, L., Ma, J., Guo, J., Tan, J., Dong, A., He, K., Zhou, J., Cinar, R., Wu, J., Salinas, A. G., Sun, L., Kumar, M., Sullivan, B. T., Oldham, B. B., Pitz, V., ... Tang, B. (2022). Deficiency in endocannabinoid synthase DAGLB contributes to early onset Parkinsonism and murine nigral dopaminergic neuron dysfunction. *Nature Communications*, 13, 3490. <https://doi.org/10.1038/s41467-022-31168-9>
- Lu, H.-C., & Mackie, K. (2016). An introduction to the endogenous cannabinoid system. *Biological Psychiatry*, 79, 516–525. <https://doi.org/10.1016/j.biopsych.2015.07.028>
- Lu, H.-C., & Mackie, K. (2021). Review of the endocannabinoid system. *Biological Psychiatry: Cognitive Neuroscience and Neuroimaging*, 6, 607–615. <https://doi.org/10.1016/j.bpsc.2020.07.016>
- Malamas, M. S., Lamani, M., Farah, S. I., Mohammad, K. A., Miyabe, C. Y., Weerts, C. M., Speziale, M., Hilston, S., Zvonok, N., Chandrashekhar, H., Ploss, M., Straiker, A., & Makriyannis, A. (2021). Design and synthesis of highly potent and specific ABHD6 inhibitors. *ChemMedChem*, 18, 116244. <https://doi.org/10.1016/j.bmc.2021.116244>
- Marrs, W. R., Blankman, J. L., Horne, E. A., Thomazeau, A., Lin, Y. H., Coy, J., Bodor, A. L., Muccioli, G. G., Hu, S. S. J., Woodruff, G., Fung, S., Lafourcade, M., Alexander, J. P., Long, J. Z., Li, W., Xu, C., Möller, T., Mackie, K., Manzoni, O. J., ... Stella, N. (2010). The serine hydrolase ABHD6 controls the accumulation and efficacy of 2-AG at cannabinoid receptors. *Nature Neuroscience*, 13, 951–957. <https://doi.org/10.1038/nn.2601>
- Michel, A. D., & Fonfria, E. (2007). Agonist potency at P2X7 receptors is modulated by structurally diverse lipids. *British Journal of Pharmacology*, 152, 523–537. <https://doi.org/10.1038/sj.bjp.0707417>
- Miras-Portugal, M. T., Diaz-Hernandez, J. I., Gomez-Villafuertes, R., Diaz-Hernandez, M., Artalejo, A. R., & Gualix, J. (2015). Role of P2X7 and P2Y2 receptors on  $\alpha$ -secretase-dependent APP processing: Control of amyloid plaques formation “in vivo” by P2X7 receptor. *Computational and Structural Biotechnology Journal*, 13, 176–181. <https://doi.org/10.1016/j.csbj.2015.02.005>
- Mitirattanakul, S., Ramakul, N., Guerrero, A. V., Matsuka, Y., Ono, T., Iwase, H., Mackie, K., Faull, K. F., & Spigelman, I. (2006). Site-specific increases in peripheral cannabinoid receptors and their endogenous ligands in a model of neuropathic pain. *Pain*, 126, 102–114. <https://doi.org/10.1016/j.pain.2006.06.016>
- Muñoz, M. F., Griffith, T. N., & Contreras, J. E. (2021). Mechanisms of ATP release in pain: Role of pannexin and connexin channels. *Purinergic Signal*, 17, 549–561. <https://doi.org/10.1007/s11302-021-09822-6>
- North, R. A., & Surprenant, A. (2000). Pharmacology of cloned P2X receptors. *Annual Review of Pharmacology and Toxicology*, 40, 563–580. <https://doi.org/10.1146/annurev.pharmtox.40.1.563>
- Ogasawara, D., Deng, H., Viader, A., Baggelaar, M. P., Breman, A., den Dulk, H., van den Nieuwendijk, A. M. C. H., Soethoudt, M., van der Wel, T., Zhou, J., Overkleeft, H. S., Sanchez-Alavez, M., Mori, S., Nguyen, W., Conti, B., Liu, X., Chen, Y., Liu, Q. S., Cravatt, B. F., & van der Stelt, M. (2016). Rapid and profound rewiring of brain lipid signaling networks by acute diacylglycerol lipase inhibition. *Proceedings of the National Academy of Sciences of the United States of America*, 113, 26–33. <https://doi.org/10.1073/pnas.1522364112>
- Percie du Sert, N., Hurst, V., Ahluwalia, A., Alam, S., Avey, M. T., Baker, M., Browne, W. J., Clark, A., Cuthill, I. C., Dirnagl, U., Emerson, M., Garner, P., Holgate, S. T., Howells, D. W., Karp, N. A., Lazic, S. E., Lidster, K., MacCallum, C. J., Macleod, M., ... Würbel, H. (2020). The ARRIVE guidelines 2.0: Updated guidelines for reporting animal research. *PLoS Biology*, 18(7), e3000410. <https://doi.org/10.1371/journal.pbio.3000410>
- Powis, G., Seewald, M. J., Gratas, C., Melder, D. C., Riebow, J. F., & Modest, E. J. (1992). Selective inhibition of phosphatidylinositol phospholipase C by cytotoxic ether lipid analogues. *Cancer Research*, 52(10), 2835–2840.
- Rassendren, F., Buell, G. N., Virginio, C., Collo, G., North, R. A., & Surprenant, A. (1997). The permeabilizing ATP receptor, P2X7. Cloning and expression of a human cDNA. *The Journal of Biological Chemistry*, 272, 5482–5486. <https://doi.org/10.1074/jbc.272.9.5482>
- Ravotto, L., Duffet, L., Zhou, X., Weber, B., & Patriarchi, T. (2020). A bright and colorful future for G-protein coupled receptor sensors. *Frontiers in Cellular Neuroscience*, 14, 67. <https://doi.org/10.3389/fncel.2020.00067>
- Reigada, D., Navarro-Ruiz, R. M., Caballero-López, M. J., Del Águila, Á., Muñoz-Galdeano, T., Maza, R. M., & Nieto-Díaz, M. (2017). Diadenosine tetraphosphate (Ap(4)A) inhibits ATP-induced excitotoxicity: A neuroprotective strategy for traumatic spinal cord injury treatment. *Purinergic Signal*, 13, 75–87. <https://doi.org/10.1007/s11302-016-9541-4>
- Ren, W. J., & Illes, P. (2022). Involvement of P2X7 receptors in chronic pain disorders. *Purinergic Signal*, 18, 83–92. <https://doi.org/10.1007/s11302-021-09796-5>
- Rinaldi-Carmona, M., Barth, F., Héaulme, M., Shire, D., Calandra, B., Congy, C., Martinez, S., Maruani, J., Néliat, G., Caput, D., Ferrara, P., Soubrié, P., Brelière, J. C., & le Fur, G. (1994). SR141716A, a potent and selective antagonist of the brain cannabinoid receptor. *FEBS Letters*, 350, 240–244. [https://doi.org/10.1016/0014-5793\(94\)00773-X](https://doi.org/10.1016/0014-5793(94)00773-X)

- Rodrigues, R. J., Tomé, A. R., & Cunha, R. A. (2015). ATP as a multi-target danger signal in the brain. *Frontiers in Neuroscience*, 9, 148.
- Sano, A., Zhu, X., Sano, H., Muñoz, N. M., Boetticher, E., & Leff, A. R. (2001). Regulation of eosinophil function by phosphatidylinositol-specific PLC and cytosolic PLA(2). *American Journal of Physiology. Lung Cellular and Molecular Physiology*, 281, L844–L851. <https://doi.org/10.1152/ajplung.2001.281.4.L844>
- Shim, J.-Y., Bertalovitz, A. C., & Kendall, D. A. (2011). Identification of essential cannabinoid-binding domains: Structural insights into early dynamic events in receptor activation. *The Journal of Biological Chemistry*, 286, 33422–33435. <https://doi.org/10.1074/jbc.M111.261651>
- Shonesy, B. C., Winder, D. G., Patel, S., & Colbran, R. J. (2015). The initiation of synaptic 2-AG mobilization requires both an increased supply of diacylglycerol precursor and increased postsynaptic calcium. *Neuropharmacology*, 91, 57–62. <https://doi.org/10.1016/j.neuropharm.2014.11.026>
- Singh, S., Sarroza, D., English, A., McGrory, M., Dong, A., Zweifel, L., Land, B. B., Li, Y., Bruchas, M. R., & Stella, N. (2023). Pharmacological characterization of the endocannabinoid sensor GRAB (eCB2.0). *Cannabis and Cannabinoid Research*, Online ahead of print. <https://doi.org/10.1089/can.2023.0036>
- Sink, K. S., McLaughlin, P. J., Wood, J. A., Brown, C., Fan, P., Vemuri, V. K., Pang, Y., Olzewska, T., Thakur, G. A., Makriyannis, A., Parker, L. A., & Salamone, J. D. (2008). The novel cannabinoid CB1 receptor neutral antagonist AM4113 suppresses food intake and food-reinforced behavior but does not induce signs of nausea in rats. *Neuropsychopharmacology*, 33, 946–955. <https://doi.org/10.1038/sj.npp.1301476>
- Slivicki, R. A., Iyer, V., Mali, S. S., Garai, S., Thakur, G. A., Crystal, J. D., & Hohmann, A. G. (2020). Positive allosteric modulation of CB1 cannabinoid receptor signaling enhances morphine antinociception and attenuates morphine tolerance without enhancing morphine-induced dependence or reward. *Frontiers in Molecular Neuroscience*, 13, 54. <https://doi.org/10.3389/fnmol.2020.00054>
- Steffens, M., Zentner, J., Honegger, J., & Feuerstein, T. J. (2005). Binding affinity and agonist activity of putative endogenous cannabinoids at the human neocortical CB1 receptor. *Biochemical Pharmacology*, 69, 169–178. <https://doi.org/10.1016/j.bcp.2004.08.033>
- Stella, N., Schweitzer, P., & Piomelli, D. (1997). A second endogenous cannabinoid that modulates long-term potentiation. *Nature*, 388, 773–778. <https://doi.org/10.1038/42015>
- Tanaka, M., Sackett, S., & Zhang, Y. (2020). Endocannabinoid modulation of microglial phenotypes in neuropathology. *Frontiers in Neurology*, 11, 87. <https://doi.org/10.3389/fneur.2020.00087>
- Thompson, A., Mostafapour, S., Denlinger, L., Bleasdale, J., & Fisher, S. (1991). The aminosteroid U-73122 inhibits muscarinic receptor sequestration and phosphoinositide hydrolysis in SK-N-SH neuroblastoma cells. A role for G<sub>p</sub> in receptor compartmentation. *Journal of Biological Chemistry*, 266, 23856–23862. [https://doi.org/10.1016/S0021-9258\(18\)54362-3](https://doi.org/10.1016/S0021-9258(18)54362-3)
- Walter, L., Dinh, T., & Stella, N. (2004). ATP induces a rapid and pronounced increase in 2-arachidonoylglycerol production by astrocytes, a response limited by monoacylglycerol lipase. *The Journal of Neuroscience*, 24, 8068–8074. <https://doi.org/10.1523/JNEUROSCI.2419-04.2004>
- Wang, X., Arcuino, G., Takano, T., Lin, J., Peng, W. G., Wan, P., Li, P., Xu, Q., Liu, Q. S., Goldman, S. A., & Nedergaard, M. (2004). P2X7 receptor inhibition improves recovery after spinal cord injury. *Nature Medicine*, 10, 821–827. <https://doi.org/10.1038/nm1082>
- Witting, A., Walter, L., Wacker, J., Moller, T., & Stella, N. (2004). P2X7 receptors control 2-arachidonoylglycerol production by microglial cells. *Proceedings of the National Academy of Sciences of the United States of America*, 101, 3214–3219. <https://doi.org/10.1073/pnas.0306707101>
- Wu, P.-Y., Lin, Y.-C., Chang, C.-L., Lu, H.-T., Chin, C.-H., Hsu, T.-T., Chu, D., & Sun, S. H. (2009). Functional decreases in P2X7 receptors are associated with retinoic acid-induced neuronal differentiation of Neuro-2a neuroblastoma cells. *Cellular Signalling*, 21, 881–891. <https://doi.org/10.1016/j.cellsig.2009.01.036>
- Young, M. T., Pelegrin, P., & Surprenant, A. (2007). Amino acid residues in the P2X7 receptor that mediate differential sensitivity to ATP and BzATP. *Molecular Pharmacology*, 71, 92–100. <https://doi.org/10.1124/mol.106.030163>
- Zou, S., & Kumar, U. (2018). Cannabinoid receptors and the endocannabinoid system: Signaling and function in the central nervous system. *International Journal of Molecular Sciences*, 19, 833. <https://doi.org/10.3390/ijms19030833>

## SUPPORTING INFORMATION

Additional supporting information can be found online in the Supporting Information section at the end of this article.

**How to cite this article:** Singh, S., Sarroza, D., English, A., Whittington, D., Dong, A., Malamas, M., Makriyannis, A., van der Stelt, M., Li, Y., Zweifel, L., Bruchas, M. R., Land, B. B., & Stella, N. (2024). P2X<sub>7</sub> receptor-dependent increase in endocannabinoid 2-arachidonoyl glycerol production by neuronal cells in culture: Dynamics and mechanism. *British Journal of Pharmacology*, 1–19. <https://doi.org/10.1111/bph.16348>